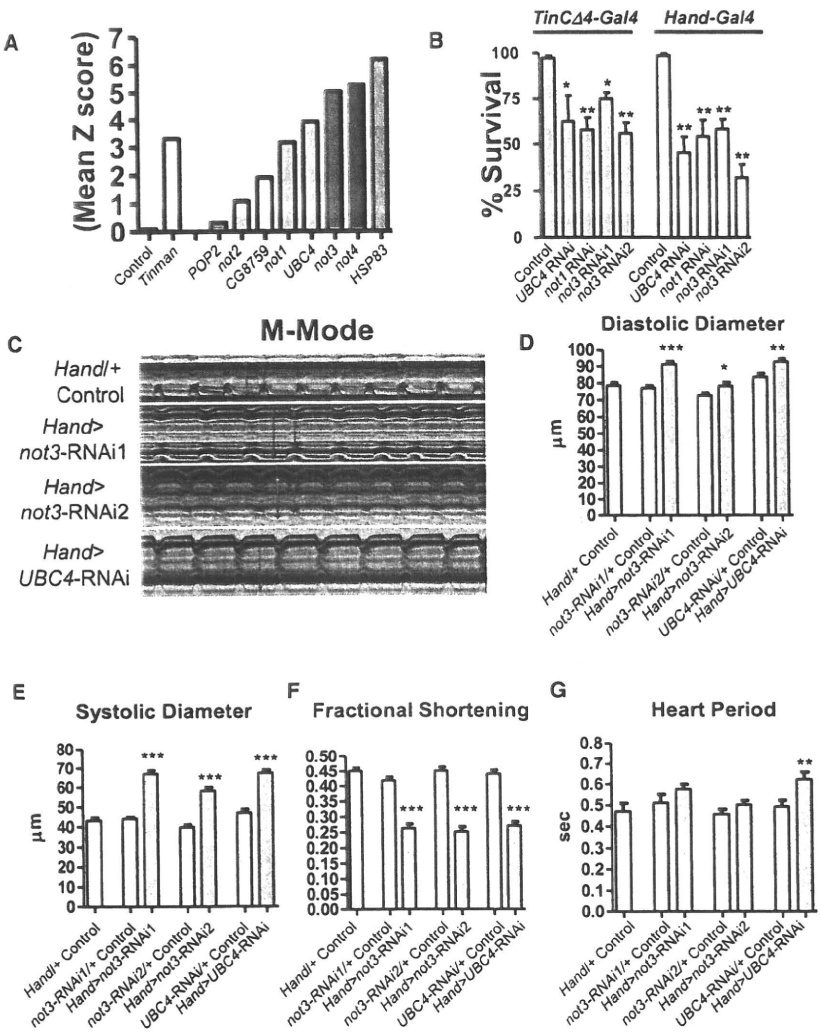

Figure 3. The CCR4-Not Complex Is a Central Regulator of Adult Heart Function, and Loss of not3 Results in Dilated Cardiomyopathy in *Drosophila*

(A) Mean Z scores for *TinCΔ4-Gal4* x *UAS*-RNAi lines targeting the indicated members of the fly CCR4-Not complex. A negative control (w^{1118} [isogenic to the RNAi library] X *TinΔ4-Gal4*) and the positive control *Tinman* RNAi line are shown.

(B) *not1*, *not3*, and *UBC4* are essential for proper adult heart function in both *Tinman*- and *Hand*-expressing cells. Data are shown as mean ± SEM for at least three replicates. RNAi1 and RNAi2 indicate different transgenic hairpins targeting *not3* . *p < 0.05, **p < 0.01 by ANOVA.

(C) One-week-old adult flies with *Hand-Gal4* driving *not3* or *UBC4* cardiac-specific knockdown exhibit impaired heart function. M modes provide traces of the heart contractions to document the movements in a 1 pixel wide region of the heart tube over time. *HandG4/+* control are the progeny of *Hand-Gal4* crossed to w^{1118}. *Hand>Not3* complex flies are the progeny of *Hand-Gal4* crossed to either *UAS-not3*-RNAi (−1 or −2) or to UAS-*UBC4*-RNAi lines. Fly heart analysis was performed with a MatLab-based image analysis program (Fink et al., 2009; Ocorr et al., 2007b). M modes of the RNAi knockdown hearts reveal dilated diastolic and systolic diameters (double-headed red arrows) and reduced shortening properties (difference between diameters) when compared to M modes of control hearts. Each trace represents a 5 s recording.

(D–G) *Not3* or *UBC4* heart-specific knockdown perturbs several indices of cardiac performance. Progeny of *Hand-Gal4* crossed to two different *UAS-not3*-RNAi lines or an *UAS-UBC4*-RNAi line (experimental) and w^{1118} crossed to *UAS*-RNAi or *Hand-Gal4* driver (controls) were used for these experiments as in (C). *not3* and *UBC4* knockdown led to significantly wider diastolic (D) and systolic (E) diameters, and as a result significantly depressed (F) fractional shortening in all experimental lines relative to controls. *not3* knockdown trended toward a slight lengthening in the heart period (time between consecutive diastolic intervals), while *UBC4* knockdown led to a significant increase in heart period (G). Mean values ± SEM are shown for each group (n = 29–40). Unpaired t tests were performed between each *Hand-Gal4>UAS*-RNAi and each corresponding *UAS*-RNAi/+ control (progeny of w^{1118} crossed to *UAS*-RNAi line). Additionally, one-way ANOVAs with Bonferroni multiple comparison tests revealed no significant differences between the *HandG4/+* control and all *UAS*-RNAi/+ control lines, for any cardiac parameter measured.

*p < 0.05, **p < 0.01, ***p < 0.001. See also Figure S3 and Movie S1.

have not yet been associated with cardiovascular function. We therefore retested components of this pathway using *TinCΔ4-Gal4*-driven knockdown in the heart, which confirmed the phenotype (Figure 3B). Moreover, use of a second heart driver, *Hand-Gal4*, which is expressed with high specificity in myocardial and pericardial cells throughout development and in the adult fly heart (Han and Olson, 2005), showed that silencing of *not1*, *not3*, and *UBC4* resulted in early death when adult flies were shifted to 29°C (Figure 3B).

Since *not3* RNAi gave a strong phenotype with two different *UAS*-RNAi lines (Figure 3B), we focused on the CCR4-Not component *not3*. Cardiac-specific knockdown of *not3* with two different RNAi lines (*Hand>not3*-RNAi: progeny from *Hand*-Gal4 crossed to *UAS-not3*-RNAi) significantly increased both diastolic and systolic diameters and resulted in reduced systolic fractional shortening relative to control flies (Figures 3C–3F and Movie S1). Hearts with cardiac *not3* knockdown also showed slight increases in heart periods (Figure 3G); however, this was not statistically significant. Fluorescent microscopy revealed that *not3* RNAi lines exhibit marked myofibrillar disarray, especially in the conical chamber (Figures 4A–4D). Heart-restricted *not3*-RNAi-mediated knockdown was confirmed by qRT-PCR (Figure S3). In addition, we observed transcriptional downregulation of the Sarcoplasmic/endoplasmic reticulum calcium ATPase

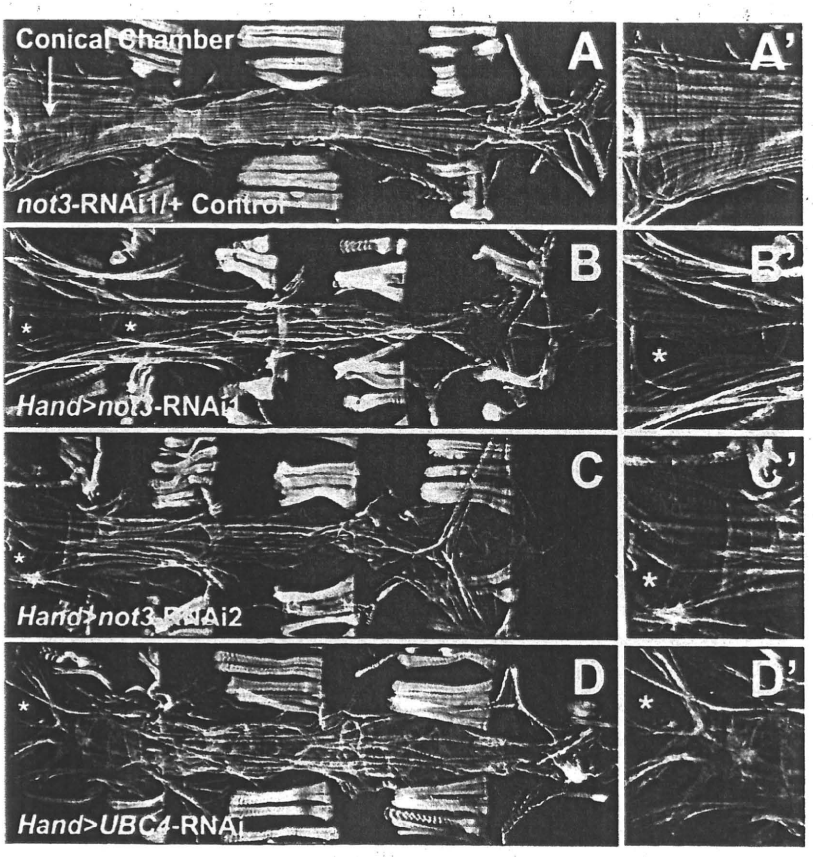

Figure 4. *not3* and *UBC4* Cardiac-Specific RNAi Knockdown Substantially Perturb Myofibrillar Organization and Content

(A) Alexa584-phalloidin staining of control *Drosophila* cardiac tubes reveals typical spiraling myofibrillar arrangements within the cardiomyocytes. The fibers, especially those in the conical chamber, located anteriorly, are densely packed with F-actin.

(B–D) Relative to control hearts, *not3* or *UBC4* RNAi knockdown severely disrupts myofibrillar organization and leads to an apparent loss of myofilaments as noted by large gaps in F-actin staining (*) as well as by a lack of myosin heavy chain transcripts (Figure S3F).

(A′–D′) Enlarged images of the conical chambers from (A)–(D), respectively, which illustrate the high degree of myofibrillar disarray and large gaps in F-actin staining within the cardiomyocytes of *not3* and *UBC4* RNAi knockdown hearts. Original images were taken at 10× magnification with a Zeiss Imager Z1 fluorescent microscope.

(*Serca2a*, *ATP2A2*), myosin heavy chain (*mhc*, *MYH7*), and the potassium channel *KCNQ* (*kcnq1*, *KCNQ1*) (Figure S3) involved in heart rhythm control. Cardiac-specific knockdown of *not3* increased the number of flies exhibiting contractile irregularities (Figures S3H and S3I), a finding similar to what is seen in response to cardiac-specific knockdown of the *KCNQ* K^+ channel (Figure S3I) and what has been reported for *KCNQ* mutant flies (Ocorr et al., 2007b). Of note, a *not3 P* element mutant was developmentally lethal, exhibiting a late stage defect in embryonic heart tube organization, which could be rescued by *P* element excision (Figure S3C).

The CCR4-Not complex component *UBC4* was also a major hit identified by our heart screen. Moreover, *UBC4* expression was reduced after *not3* knockdown (Figure S3B). *Hand-Gal4>UAS-UBC4*-RNAi flies also exhibited significantly longer heart periods and showed dramatically altered diastolic and systolic diameters and reduced fractional shortening relative to control hearts (Figures 3C–3G). Fluorescent imaging again revealed severe myofibrillar disarray (Figure 4D) that was strikingly similar to that observed in *not3* knockdown hearts. Further, we observed similar structural and functional phenotypes in *not1* cardiac-specific knockdown flies (A.C., G.N., J.P., and R.B., unpublished data). Thus, knockdown of different components of the CCR4-Not complex result in abnormal heart structure and severely impaired cardiac function indicative of dilated cardiomyopathy.

Functional Assessment of Additional *Drosophila* Heart Hits

To extend our confirmations beyond the CCR4-Not complex, we assayed heart function in adult flies with heart-specific knockdown of four additional candidates identified in our heart screen (Figure S3). One candidate heart gene tested was *CG1216* (*Mrityu*), which encodes a mesoderm-expressed BTB-POZ domain-containing protein (Rusconi and Challa, 2007). Cardiac knockdown of *CG1216* resulted in a significant increase in systolic diameter. Another candidate heart gene, *CG8933* (*extradenticle*), encodes a PBX-family transcription factor. Cardiac knockdown of *CG8933* resulted in increased systolic diameter and reduced fractional shortening. Cardiac knockdown of *CG33261* (*Trithorax-like*) resulted in significantly altered diastolic and systolic diameters as well as impaired fractional shortening. Finally, knockdown of *CG7371*, which encodes a Vps52 domain-containing protein predicted to participate in Golgi trafficking, resulted in a marked increase in heart period and affected the diastolic diameter. These data further demonstrate that our screen indeed has the capacity to identify novel factors involved in and required for normal adult heart function.

Generation of *not3* Knockout Mice

We next tested whether our data on *Drosophila* can be directly translated into a mammalian species. The mouse and human NOT3 proteins (official gene name *Cnot3*) share 60% identity with the *Drosophila not3* ortholog. Expression of human and mouse *not3* messenger RNA (mRNA) transcripts can be found in the majority of tissues analyzed. Although *not3* is evolutionarily conserved from yeast to mammals, essentially nothing is known about the in vivo role of mammalian *not3*. We therefore generated *not3* knockout mice.

We disrupted the *not3* gene in murine embryonic stem cells (ESCs) using a targeting vector in which nucleotides encompassing exons 2 through 9 are deleted (Figure 5A and Figure S4A). Both $not3^{+/-}$ male and $not3^{+/-}$ female mice are viable and exhibit normal fertility. We never obtained viable $not3^{-/-}$ newborn mice, indicating that loss of *not3* results in embryonic lethality. We staged embryonic development but failed to recover *not3* null embryos from placental implantations (Figures S4B and S4C). We therefore assayed early embryogenesis and observed that $not3^{-/-}$ blastocysts can develop. These mutant blastocysts have a normal appearance (Figure S4D), occur at Mendelian frequencies (Figures S4E and S4F), and express key markers of early embryonic differentiation at normal levels (Figure S4G). *not3* mRNA transcripts and NOT3 protein were undetectable in $not3^{-/-}$ blastocysts by RT-PCR and immunostaining (Figures S4F and S4G). In $not3^{+/+}$ and $not3^{-/-}$ epiblast cultures (Figure S4H), trophoblast cells started to spread and supported the outgrowths of the inner cell mass (ICM). While the ICM of $not3^{+/+}$ blastocysts continued to grow, $not3^{-/-}$ ICM cells exhibited a severe outgrowth defect. Thus, complete loss of mouse *not3* results in early embryonic death at the implantation stage.

not3 Haploinsufficiency Results in Impaired Heart Function

We speculated that similar to RNAi-mediated downregulation of *not3* in *Drosophila*, *not3* haploinsufficiency might also reveal a role in mammalian heart function. In *not3* heterozygote mice, *not3* expression is indeed downregulated in the heart (Figure 5B). We failed to observe overt structural changes in the hearts of $not3^{+/-}$ mice. However, both male and female *not3* haploinsufficient mice exhibited a reduction in cardiac contractility as determined by decreased left ventricle fractional shortening and increased left ventricular diameter in systole (Figures 5C and 5D).

To address whether the defects in cardiac function are intrinsic to the heart per se or whether the observed impairment of contractility was secondary because of haploinsufficiency of *not3* in other tissues, we subjected explanted hearts from wild-type and $not3^{+/-}$ littermate mice to Langendorff perfusion, assessing ex vivo heart function (Joza et al., 2005). When isoproterenol was used to activate β-adrenergic receptors, $not3^{+/-}$ hearts exhibited severe contractile abnormalities as defined by impaired generation of left ventricular pressure (LVP) (Figure 5E and Figure S5A). Hemodynamic measurements confirmed that all functional heart parameters such as dP/dT_{max} or dP/dT_{min}, indicative of generated contractile pressure, were markedly reduced in $not3^{+/-}$ hearts (data not shown). Moreover, when explanted hearts were electrically stimulated, $not3^{+/-}$ hearts exhibited a striking defect in contractility (Figure 5F). Thus, downregulation of *not3* expression in *not3* haploinsufficient mice results in an intrinsic impairment in heart function.

Yeast strains mutant for components of the CCR4-Not complex, including *not3*, display reduced acetylation levels of lysine residues on histone tails (e.g., H3K9) (Peng et al., 2008) and/or reduced trimethylation of H3K4 (Laribee et al., 2007). H3K9 acetylation and H3K4 trimethylation are indicative of transcriptionally active states of chromatin. Moreover, promoter regions of NOT3 target genes were shown to recruit trimethylated H3K4 in mouse ESCs (Hu et al., 2009), suggesting that NOT3 may regulate chromatin modifications. Our gene expression and bioinformatic analyses of mouse *not3* knockout cells revealed that histone deacetylases (HDACs) and mRNA metabolisms are localized central in gene networks (K.K., unpublished data). We therefore assessed the state of histone modifications in hearts from $not3^{+/-}$ mice. Histone extracts of whole hearts from *not3* haploinsufficient mice showed a slight but significant reduction in active histone marks such as acetylation of H3K9 and trimethylation of H3K4 (Figures 5G and 5H and Figure S5). H3K27 trimethylation was not changed (Figure 5I and Figure S5). Treatment of $not3^{+/-}$ hearts with the HDAC inhibitor VPA restored the reduced acetylation of H3K9 and H3K4 trimethylation to that of wild-type levels (Figures 5G–5I and Figure S5). Most importantly, administration of HDAC inhibitors rescued the impairment in heart function in $not3^{+/-}$ mice; i.e., ex vivo heart functions of VPA treated mice were similar to control mice in response to both isoproterenol (Figure 5J) and electrical stimulation (Figure 5K). These data were confirmed with TSA, a second HDAC inhibitor (Figures S5H and S5I). Together, these data show that $not3^{+/-}$ mice exhibit a spontaneous and intrinsic defect in cardiac function that can be rescued with HDAC inhibitors.

$not3^{+/-}$ Mice Develop Severe Cardiomyopathy in Response to Cardiac Stress

We next exposed control and $not3^{+/-}$ littermates to chronic pressure overload by surgical constriction of the aorta (transverse aortic constriction, TAC). Three weeks after TAC, heart weight/body weight ratios (HW/BW) increased in both $not3^{+/+}$ and $not3^{+/-}$ mice, although this increase was significantly larger in the $not3^{+/-}$ mice (Figure 6A). Cardiac hypertrophy was also seen by histology (Figure 6D and Figure S6A). Aortic banding of $not3^{+/-}$ mice resulted in severe heart failure characterized by decreased fractional shortening (Figure 6B) and a dilation of the left ventrical as determined by echocardiography (Figure 6C). In addition, $not3^{+/-}$ mice develop severe cardiac fibrosis after TAC, as shown by Masson-trichrome staining of hearts 3 weeks after TAC (Figure 6D and Figure S6B). Thus, $not3^{+/-}$ mice develop severe symptoms of heart failure in response to cardiac stress.

We next assessed whether HDAC inhibitors can also rescue stress-induced heart failure. HDAC inhibitor treatment could indeed block the augmented loss of cardiac function observed in $not3^{+/-}$ mice after TAC (Figures 7A and 7B). In vivo treatment of $not3^{+/-}$ mice with HDAC inhibitors also blocked the exaggerated induction of heart failure markers such as *ANF* (Figure S6C) and *βMyhc* (Figure S6D). Moreover, treatment with an HDAC inhibitor restored the observed histone alterations in $not3^{+/-}$ mice to that of wild-type littermates (Figure 7C and Figures S6E and S6F). Thus, *not3* haploinsufficiency results in exaggerated heart failure that can be rescued by HDAC inhibition in vivo.

A Common Genomic Variant in the *NOT3* Promoter Correlates with Cardiac Repolarization Duration in Humans

Using an in silico search to identify NOT3 target genes, we found that NOT3 has been shown to bind to the *Kcnq1* promoter in

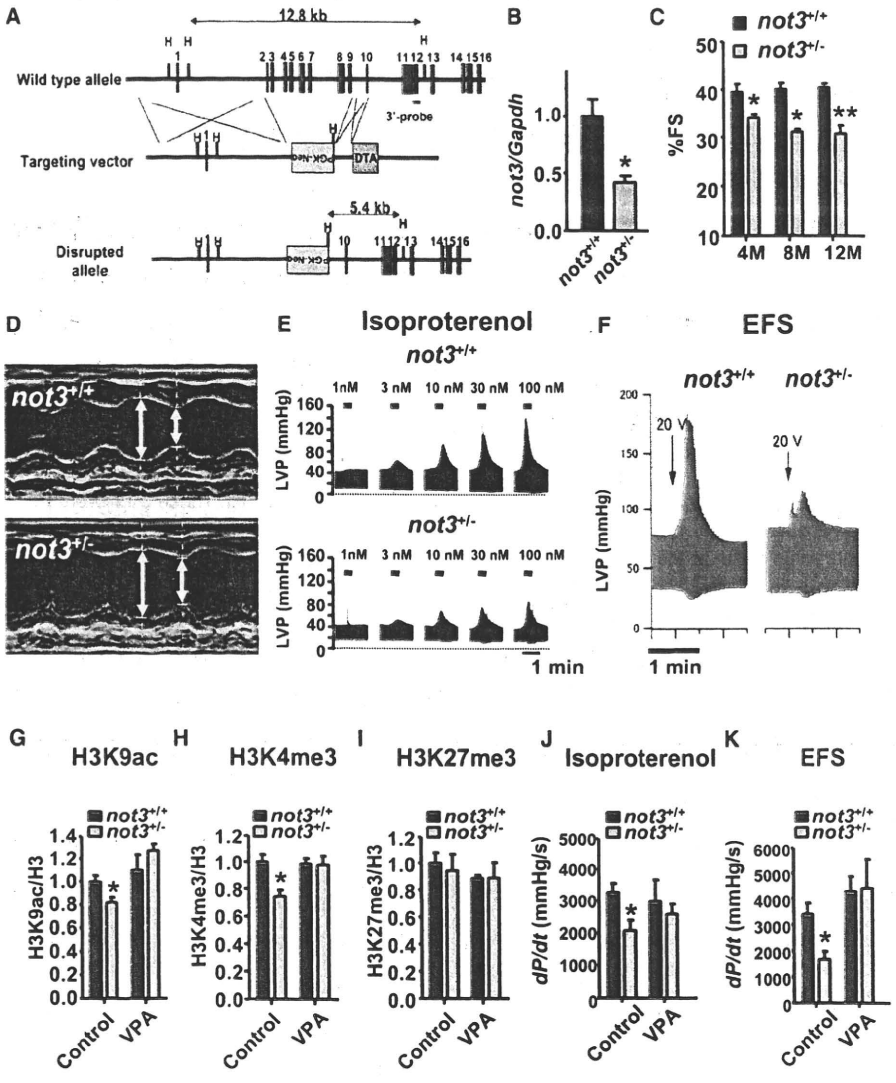

Figure 5. *not3*$^{+/-}$ Mice Exhibit Reduced Heart Contractility, Ex Vivo Function, and Histone Modifications that Can Be Rescued by Treatment with HDAC Inhibitors

(A) Gene targeting strategy. Exons 2 to 9 of the *not3* gene (official symbol *cnot3*) were replaced with a PGK-Neo cassette by homologous recombination in A9 ESCs. The wild-type allele, targeting vector, mutant allele, and PGK-Neo and DTH selection cassettes are shown. Blue boxes indicate exons.

(B) Real-time PCR analyses for *not3* mRNA expression in 3-month-old wild-type and *not3*$^{+/-}$ hearts. Values were normalized to *gapdh* mRNA expression. n = 6 mice per group.

(C) *not3*$^{+/-}$ mice display a significant reduction in percent fractional shortening at 4 months of age, which became more pronounced with age. n = 6–8 mice per group. Fractional shortening was determined by echocardiography.

(D) Representative M mode echocardiography for wild-type and *not3*$^{+/-}$ mice at 8 months of age.

(E) Left ventricular pressure (LVP) measurements in isolated ex vivo *not3*$^{+/-}$ and *not3*$^{+/+}$ hearts under isoproterenol perfusion. *not3*$^{+/-}$ hearts from 4-month-old mice showed impaired contractile responses to different doses of isoproterenol perfusion in the retrograde Langendorff mode as compared to age-matched controls.

(F) Impaired contractile response of ex vivo *not3*$^{+/-}$ hearts to electrical field stimulation (EFS) compared with littermate *not3*$^{+/+}$ hearts. Representative data for left ventricular pressure (LVP) at 20 V stimulation are shown.

(G–I) H3K9 acetylation (H3K9ac) (G), H3K4 trimethylation (H3K4me3) (H), and H3K27 trimethylation (H3K27me3) (I) levels were analyzed by western blot for acid-extracted histones from whole heart ventricles of wild-type and *not3*$^{+/-}$ mice treated with vehicle or VPA (0.71% w/v in drinking water for 1 week) Band intensities were normalized to total H3 levels.

(J and K) Treatment (1 week) with the HDAC inhibitor VPA rescue impaired ex vivo heart contractility of *not3*$^{+/-}$ hearts to isoproterenol (100 nM) perfusion or 25 V EFS.

All values are mean ± SEM. *$p < 0.05$; **$p < 0.01$. n = 5–12 per group. See also Figures S4 and S5.

mammalian species and, in combination with other genome-wide approaches, can reveal regulators of heart function and heart failure.

EXPERIMENTAL PROCEDURES

Detailed experimental procedures are provided in the Extended Experimental Procedures.

Fly Stocks

All RNAi transgenic fly lines were obtained from the Vienna *Drosophila* RNAi Center (VDRC) RNAi stocks (Dietzl et al., 2007). The cardiac tissue-specific *TinCΔ4 12a-Gal4* was a kind gift from Manfred Frasch, (Lo and Frasch, 2001) and *Hand-Gal4* was a gift from Eric Olsen (Han and Olson, 2005).

Screening System

Transgenic RNAi males were crossed to *TinCΔ4* virgin females. Viable lines were then incubated at 29°C for 6 days to expose flies to temperature stress (Paternostro et al., 2001). Initially, a Z score cutoff of 2 (mean control-test)/SD was used to select RNAi lines for retesting.

Drosophila Cardiac Function, Morphology, and Gene Expression

UAS-RNAi fly lines obtained from the Vienna *Drosophila* RNAi Center were crossed to *Hand-Gal4* (II) driver flies and to w^{1118} wild-type control flies. Flies were assessed for heart morphology and physiology with high-speed digital video imaging (Ocorr et al., 2007b). M modes were generated and cardiac parameters including heart periods, diastolic and systolic diameters, and fractional shortening were recorded for each group with a MatLab-based image analysis program (Fink et al., 2009). Fluorescent imaging of *Drosophila* heart tubes was performed as described (Alayari et al., 2009).

Bioinformatics Analysis

For a detailed description of full bioinformatics analysis, please see the Extended Experimental Procedures.

Phenotyping of *not3* Knockout Mice

A targeting vector was constructed to replace exons 2 and 9 of the murine *not3* gene. Fractional shortening (FS) was calculated as follows: FS = [(LVEDD − LVESD)/LVEDD] × 100. For ex vivo heart studies, hearts were assayed with a Langendorff apparatus. The heart was paced electrically at 400 beats/min (bpm), and the electrical field stimulation (EFS) was applied in conjunction with the pacing stimulation. Isoproterenol was perfused for 30 s with the indicated doses. For HDAC inhibition, wild-type and $not3^{+/-}$ mice were treated with vehicle, Trichostatin A (TSA), or Valproic acid (VPA) for 1 week. Acid-extracted histones were prepared, resolved, and transferred to nitrocellulose membranes for western blotting. Transverse aorta constriction (TAC) was performed as described (Kuba et al., 2007). For heart histology, hearts were arrested, fixed, embedded in paraffin, and stained with hematoxylin and eosin (H&E) or Masson-Trichrome.

Human QT Interval Association

Human QT interval association signals over the NOT3 region were obtained from data generated by the QTSCD Consortium (Pfeufer et al., 2009).

SUPPLEMENTAL INFORMATION

Supplemental Information includes Extended Experimental Procedures, six figures, five tables, and one movie and can be found with this article online at doi:10.1016/j.cell.2010.02.023.

ACKNOWLEDGMENTS

We thank all members of our laboratories and the VDRC, the Bioscience Education Research Center (Akita University), and Vincent Chen for helpful discussions and excellent technical support. We thank Eric Olson for the *Hand-Gal4* driver and Manfred Frasch for *TinCΔ4-Gal4* driver stocks. We thank the members of the QTSCD consortium for valuable support and discussion. J.M.P. is supported by the IMBA, the Austrian Ministry of Science, a European Research Council Advanced Investigator grant, and EuGeneHeart. K.K. is supported by Kaken (21659198) from the Japanese Ministry of Science, the Medical Top Track Program, and the Japan Heart Foundation. G.G.N. was supported by a Marie Curie International Incoming Fellowship. A.C. was supported by a postdoctoral fellowship and K.O. by a Scientist Development Grant from the American Heart Association. R.B. was supported by grants from the National Heart, Lung, and Blood Institute of the National Institutes of Health. A.P. is supported by grants 01GR0803 and 01EZ0874 from the German Federal Ministry of Research, FSID-261/2008 from the UK Foundation for the Study of Infant Deaths, and YGEIA/1104/17 and ERYEX/0406/06 from the Cyprus Cardiovascular Disease Educational and Research Trust. Y.I. is supported by the Global Center of Excellence Program.

Received: May 4, 2009
Revised: October 20, 2009
Accepted: February 2, 2010
Published: April 1, 2010

REFERENCES

A.H.A. (2005). http://www.americanheart.org/.

Alayari, N.N., Vogler, G., Taghli-Lamallem, O., Ocorr, K., Bodmer, R., and Cammarato, A. (2009). Fluorescent Labeling of *Drosophila* Heart Structures. J. Vis. Exp. 10.3791/1423.

Albert, T.K., Lemaire, M., van Berkum, N.L., Gentz, R., Collart, M.A., and Timmers, H.T. (2000). Isolation and characterization of human orthologs of yeast CCR4-NOT complex subunits. Nucleic Acids Res. *28*, 809–817.

Behm-Ansmant, I., Rehwinkel, J., Doerks, T., Stark, A., Bork, P., and Izaurralde, E. (2006). mRNA degradation by miRNAs and GW182 requires both CCR4:NOT deadenylase and DCP1:DCP2 decapping complexes. Genes Dev. *20*, 1885–1898.

Bodmer, R. (1995). Heart development in Drosophila and its relationship to vertebrates. Trends Cardiovasc. Med. *5*, 21–28.

Cripps, R.M., and Olson, E.N. (2002). Control of cardiac development by an evolutionarily conserved transcriptional network. Dev. Biol. *246*, 14–28.

Denis, C.L. (1984). Identification of new genes involved in the regulation of yeast alcohol dehydrogenase II. Genetics *108*, 833–844.

Dietzl, G., Chen, D., Schnorrer, F., Su, K.C., Barinova, Y., Fellner, M., Gasser, B., Kinsey, K., Oppel, S., Scheiblauer, S., et al. (2007). A genome-wide transgenic RNAi library for conditional gene inactivation in Drosophila. Nature *448*, 151–156.

Dudbridge, F., and Gusnanto, A. (2008). Estimation of significance thresholds for genomewide association scans. Genet. Epidemiol. *32*, 227–234.

Fink, M., Callol-Massot, C., Chu, A., Ruiz-Lozano, P., Izpisua Belmonte, J.C., Giles, W., Bodmer, R., and Ocorr, K. (2009). A new method for detection and quantification of heartbeat parameters in Drosophila, zebrafish, and embryonic mouse hearts. Biotechniques *46*, 101–113.

Gordon, T., Castelli, W.P., Hjortland, M.C., Kannel, W.B., and Dawber, T.R. (1977). Predicting coronary heart disease in middle-aged and older persons. The Framington study. JAMA *238*, 497–499.

Han, Z., and Olson, E.N. (2005). Hand is a direct target of Tinman and GATA factors during Drosophila cardiogenesis and hematopoiesis. Development *132*, 3525–3536.

Hu, G., Kim, J., Xu, Q., Leng, Y., Orkin, S.H., and Elledge, S.J. (2009). A genome-wide RNAi screen identifies a new transcriptional module required for self-renewal. Genes Dev. *23*, 837–848.

Jayne, S., Zwartjes, C.G., van Schaik, F.M., and Timmers, H.T. (2006). Involvement of the SMRT/NCoR-HDAC3 complex in transcriptional repression by the CNOT2 subunit of the human Ccr4-Not complex. Biochem. J. *398*, 461–467.

Joza, N., Oudit, G.Y., Brown, D., Bénit, P., Kassiri, Z., Vahsen, N., Benoit, L., Patel, M.M., Nowikovsky, K., Vassault, A., et al. (2005). Muscle-specific

loss of apoptosis-inducing factor leads to mitochondrial dysfunction, skeletal muscle atrophy, and dilated cardiomyopathy. Mol. Cell. Biol. *25*, 10261–10272.

Kuba, K., Zhang, L., Imai, Y., Arab, S., Chen, M., Maekawa, Y., Leschnik, M., Leibbrandt, A., Markovic, M., Makovic, M., et al. (2007). Impaired heart contractility in Apelin gene-deficient mice associated with aging and pressure overload. Circ. Res. *101*, e32–e42.

Lakatta, E.G., and Levy, D. (2003). Arterial and cardiac aging: major shareholders in cardiovascular disease enterprises: Part II: the aging heart in health: links to heart disease. Circulation *107*, 346–354.

Laribee, R.N., Shibata, Y., Mersman, D.P., Collins, S.R., Kemmeren, P., Roguev, A., Weissman, J.S., Briggs, S.D., Krogan, N.J., and Strahl, B.D. (2007). CCR4/NOT complex associates with the proteasome and regulates histone methylation. Proc. Natl. Acad. Sci. USA *104*, 5836–5841.

Lloyd-Jones, D., Adams, R., Carnethon, M., De Simone, G., Ferguson, T.B., Flegal, K., Ford, E., Furie, K., Go, A., Greenlund, K., et al. American Heart Association Statistics Committee and Stroke Statistics Subcommittee. (2009). Heart disease and stroke statistics—2009 update: a report from the American Heart Association Statistics Committee and Stroke Statistics Subcommittee. Circulation *119*, e21–e181.

Lo, P.C., and Frasch, M. (2001). A role for the COUP-TF-related gene seven-up in the diversification of cardioblast identities in the dorsal vessel of Drosophila. Mech. Dev. *104*, 49–60.

Morita, H., Seidman, J., and Seidman, C.E. (2005). Genetic causes of human heart failure. J. Clin. Invest. *115*, 518–526.

Moss, A.J., and Kass, R.S. (2005). Long QT syndrome: from channels to cardiac arrhythmias. J. Clin. Invest. *115*, 2018–2024.

Mudd, J.O., and Kass, D.A. (2008). Tackling heart failure in the twenty-first century. Nature *451*, 919–928.

Nabel, E.G. (2003). Cardiovascular disease. N. Engl. J. Med. *349*, 60–72.

Nerbonne, J.M. (2004). Studying cardiac arrhythmias in the mouse—a reasonable model for probing mechanisms? Trends Cardiovasc. Med. *14*, 83–93.

Newton-Cheh, C., Eijgelsheim, M., Rice, K.M., de Bakker, P.I., Yin, X., Estrada, K., Bis, J.C., Marciante, K., Rivadeneira, F., Noseworthy, P.A., et al. (2009). Common variants at ten loci influence QT interval duration in the QTGEN Study. Nature genetics *41*, 399–406.

Ocorr, K., Perrin, L., Lim, H.Y., Qian, L., Wu, X., and Bodmer, R. (2007a). Genetic control of heart function and aging in Drosophila. Trends Cardiovasc. Med. *17*, 177–182.

Ocorr, K., Reeves, N.L., Wessells, R.J., Fink, M., Chen, H.S., Akasaka, T., Yasuda, S., Metzger, J.M., Giles, W., Posakony, J.W., and Bodmer, R. (2007b). KCNQ potassium channel mutations cause cardiac arrhythmias in Drosophila that mimic the effects of aging. Proc. Natl. Acad. Sci. USA *104*, 3943–3948.

Paternostro, G., Vignola, C., Bartsch, D.U., Omens, J.H., McCulloch, A.D., and Reed, J.C. (2001). Age-associated cardiac dysfunction in Drosophila melanogaster. Circ. Res. *88*, 1053–1058.

Peng, W., Togawa, C., Zhang, K., and Kurdistani, S.K. (2008). Regulators of cellular levels of histone acetylation in Saccharomyces cerevisiae. Genetics *179*, 277–289.

Pfeufer, A., Sanna, S., Arking, D.E., Müller, M., Gateva, V., Fuchsberger, C., Ehret, G.B., Orrú, M., Pattaro, C., Köttgen, A., et al. (2009). Common variants at ten loci modulate the QT interval duration in the QTSCD Study. Nat. Genet. *41*, 407–414.

Qian, L., and Bodmer, R. (2009). Partial loss of GATA factor Pannier impairs adult heart function in Drosophila. Hum. Mol. Genet. *18*, 3153–3163.

Qian, L., Mohapatra, B., Akasaka, T., Liu, J., Ocorr, K., Towbin, J.A., and Bodmer, R. (2008). Transcription factor neuromancer/TBX20 is required for cardiac function in Drosophila with implications for human heart disease. Proc. Natl. Acad. Sci. USA *105*, 19833–19838.

Ray, V.M., and Dowse, H.B. (2005). Mutations in and deletions of the Ca2+ channel-encoding gene cacophony, which affect courtship song in Drosophila, have novel effects on heartbeating. J. Neurogenet. *19*, 39–56.

Rusconi, J.C., and Challa, U. (2007). Drosophila Mrityu encodes a BTB/POZ domain-containing protein and is expressed dynamically during development. Int. J. Dev. Biol. *51*, 259–263.

Sanguinetti, M.C., and Tristani-Firouzi, M. (2006). hERG potassium channels and cardiac arrhythmia. Nature *440*, 463–469.

Sanyal, S., Jennings, T., Dowse, H., and Ramaswami, M. (2006). Conditional mutations in SERCA, the Sarco-endoplasmic reticulum Ca2+-ATPase, alter heart rate and rhythmicity in Drosophila. J. Comp. Physiol. [B] *176*, 253–263.

Tucker, M., Valencia-Sanchez, M.A., Staples, R.R., Chen, J., Denis, C.L., and Parker, R. (2001). The transcription factor associated Ccr4 and Caf1 proteins are components of the major cytoplasmic mRNA deadenylase in Saccharomyces cerevisiae. Cell *104*, 377–386.

Wang, Q., Curran, M.E., Splawski, I., Burn, T.C., Millholland, J.M., VanRaay, T.J., Shen, J., Timothy, K.W., Vincent, G.M., de Jager, T., et al. (1996). Positional cloning of a novel potassium channel gene: KVLQT1 mutations cause cardiac arrhythmias. Nat. Genet. *12*, 17–23.

Yusuf, S., Reddy, S., Ounpuu, S., and Anand, S. (2001). Global burden of cardiovascular diseases: part I: general considerations, the epidemiologic transition, risk factors, and impact of urbanization. Circulation *104*, 2746–2753.

Developmental Biology 340 (2010) 30–40

Contents lists available at ScienceDirect

Developmental Biology

journal homepage: www.elsevier.com/developmentalbiology

Epigenetic control of cardiomyocyte production in response to a stress during the medaka heart development

Yusuke Taneda [a], Sayaka Konno [a], Shinji Makino [b], Mai Morioka [a], Keiichi Fukuda [b], Yoshiyuki Imai [a], Akira Kudo [a], Atsushi Kawakami [a,*]

[a] Department of Biological Information, Tokyo Institute of Technology, 4259 Nagatsuta, Midori-ku, Yokohama 226-8501, Japan
[b] Department of Regenerative Medicine and Advanced Cardiac Therapeutics, Keio University School of Medicine, Shinjuku, Tokyo, Japan

ARTICLE INFO

Article history:
Received for publication 12 August 2009
Revised 12 January 2010
Accepted 12 January 2010
Available online 21 January 2010

Keywords:
Medaka
Mutant
Heart development
Myosin heavy chain
Transgenic
Epigenetic regulation

ABSTRACT

The size and morphology of organs are largely determined by a genetic program. However in some cases, an epigenetic mechanism influences the process of organ development. Particularly, epigenetic factors such as hemodynamic stress and blood pressure affect the morphogenesis of cardiac chambers and valves. Here, we report that the epigenetic influences affect the cardiomyocyte production. Taking advantage of longer developmental period of medaka fish, we could examine the later emerging tissue responses to the defect of ventricular beating, which occurred in the *hozuki* (*hoz*) mutant that harbors the mutated *ventricular myosin heavy chain* (*vmhc*) gene. The mutant showed a remarkable ventricular enlargement, and we showed that this enlargement was due to an excess production of ventricular cardiomyocytes in addition to the lack of concentric chamber growth. By experimental blockade of blood flow, we demonstrated that an elevated cardiac pressure was responsible for the aberrant cardiomyocyte production. From these data, we propose that the epigenetic tissue response to a stressed situation controls the production of cardiomyocytes to attain a fine tuning of heart formation.

Introduction

The formation of a functional vertebrate heart requires processes that create proper morphology and size during embryonic development. In particular, an adequate size and wall thickness of the heart chambers are necessary for generating enough blood circulation for the growth of the animal. For this, the heart increases its cell number by cardiomyocyte proliferation, thickens the wall of its chambers by the concentric growth in a direction perpendicular to the lumen, and finally forms the highly trabeculated chambers. However, as the cardiomyocyte proliferation ceases after embryonic development, the postnatal increase in heart size occurs by the hypertrophic growth of individual cardiomyocytes, the increase in the amount of intercellular matrices, and the proliferation of non-muscle cells (Leu et al., 2001). Only recently, it was reported that a fraction of adult cardiomyocytes retain the potential for cell division (Beltrami et al., 2001; Bergmann et al., 2009), but the number of dividing cells is less than 0.0005% of total cardiomyocytes and less than 0.08% even when the heart is injured by infarcts (Soonpaa and Field, 1997). Thus, the total number of cardiomyocytes, which is critical for the heart to function as a pump, is largely determined during embryonic development; and accordingly any subtle abnormalities in cardiomyocyte proliferation and heart morphogenesis in the embryo may affect the homeostasis and function of the postnatal heart.

A number of recent studies have suggested that both paracrine factors from peripheral tissues such as the epicardium and endocardium and autocrine factors secreted from the cardiomyocyte itself support cardiomyocyte proliferation and chamber morphogenesis. The action of retinoic acid (RA) and Erythropoietin (Epo) on epicardiac cells produces paracrine growth factors such as Fibroblast growth factors (Fgf) 9, 16, and 20; and the resultant activation of downstream signaling pathways through the FGF receptor induces the proliferation of myoblasts (Lavine et al., 2005). In parallel, Bmp10 has been proposed as one of the autocrine growth factors expressed by the cardiomyocytes themselves. In *Bmp10* knockout mice, an apparent reduction in cardiomyocyte proliferation occurs, accompanied by an increase in the level of P57Kip2, an inhibitory protein against Cyclin-dependent kinase (Cdk; Chen et al., 2004). From the analysis of conditional knockout of the transcription factor Nkx2.5 in adult mice, it has been shown that Bmp10 function is also necessary for the trabecular muscle growth in postnatal stages (Pashmforoush et al., 2004). Furthermore, additional signaling pathways including the Reptin and Pontin (Rottbauer et al., 2002) and the L-type calcium channel (Rottbauer et al., 2001) are also involved in the regulation of cardiomyocyte proliferation during development. In addition to these positive regulators, a study in mice has identified a negative regulator for cardiomyocyte proliferation, Jumonji, which is required for the cessation of cardiomyocyte proliferation in postnatal stages (Toyoda

* Corresponding author. Fax: +81 45 924 5718.
E-mail address: atkawaka@bio.titech.ac.jp (A. Kawakami).

0012-1606/$ – see front matter © 2010 Elsevier Inc. All rights reserved.
doi:10.1016/j.ydbio.2010.01.014

et al., 2003). The *Jumonji* gene is expressed in stages when the active cardiomyocyte proliferation is terminated, and the mutant mice display an elevated expression of *cyclinD1* and aberrant proliferation of their cardiomyocytes.

In addition to the cardiomyocyte number, another important process for making a functional heart is the formation of its thick-layered chambers. During the early stage of heart development, a thin-layered cardiac wall grows within a planar direction; however, at an appropriate stage of heart development, the cardiomyocyte changes the polarity of cell divisions and adds new cells in the myocardium in a direction perpendicular to the lumen to attain the concentric growth. Three zebrafish mutants with defective concentric growth of heart chambers, *heart of glass*, *santa*, and *valentine*, have been isolated by a mutant screening (Mably et al., 2003; Mably et al., 2006). Analyses of them have identified a novel signaling pathway for concentric growth, in which the Heart of glass protein in the endocardium regulates the concentric growth of the myocardium. Additionally, the endocardium also plays a role in the trabeculation of the heart chambers; i.e., Neuregulin (Nrg), a molecule secreted from the endocardium, is necessary for the trabeculation by acting through its receptors, ErbB2 and ErbB4, in the myocardium (Gassmann et al., 1995; Lee et al., 1995; Meyer and Birchmeier, 1995).

Thus, cardiomyocyte proliferation and formation of a thick chamber wall are largely regulated by genetic factors. However, in addition to such genetic factors, recent studies have suggested that epigenetic factors also influence heart formation. For example, in the zebrafish mutant *weak atrium* (*wea*), which has a nonsense mutation in the *atrium myosin heavy chain* (*amhc*) gene, the ventricle formation is adversely affected due to the defective heartbeat in the atrium (Berdougo et al., 2003). The *silent heart* (*sih*)/*cardiac troponin T* and *cardiofunk* (*cfk*)/*sarcomere actin* mutants, whose heartbeat is completely impaired, show a defect in endocardial cushion (EC) formation (Sehnert et al., 2002; Bartman et al., 2004). Moreover, analysis using the *wea* and *half-hearted* (*haf*)/*ventricle myosin heavy chain* (*vmhc*) mutant zebrafish has suggested that the blood flow affects the regional cell-shape changes of cardiomyocytes and the resulting formation of the ventricular curvature (Auman et al., 2007). Thus, epigenetic factors such as the heartbeat and blood flow influence heart morphogenesis. However, it has not been documented in detail whether or not the epigenetic factors also influence other aspects of heart morphogenesis such as the cardiomyocyte production and concentric chamber growth.

Here we report that the defective ventricular heart beat in the medaka mutant *hozuki* (*hoz*), which has a nonsense mutation in the *vmhc* gene, affected the concentric chamber growth and the number of cardiomyocytes in the ventricle. We show that an elevated cardiac pressure causes the excess production of cardiomyocyte. Our data thus suggest the existence of an epigenetic response mechanism that tunes the production of ventricular cardiomyocytes in response to an altered physiological condition.

Methods

Fish strains and maintenance

Medaka fish (*Oryzias latipes*) of wild type strains, Cab and HNI, were maintained at 28.5 °C in a re-circulating system with a 14-h/day and 10-h/night cycle. The medaka heart mutant *hozuki* (*hoz*), a Japanese word meaning "ground cherry," was isolated by our previous mutant screening (Sakamoto et al., 2004). Collected fertilized eggs were incubated at 28.5 °C in medaka Ringer's solution (0.65% NaCl, 0.04% KCl, 0.011% $CaCl_2$, 0.01% $MgSO_4$, 0.01% $NaHCO_3$, and 0.0001% methylene blue), and developmental stages were determined by their morphology according to the medaka stage table described by Iwamatsu (2004).

Genetic mapping and positional cloning

Genetic mapping was performed according to the method described earlier (Kimura et al., 2005). Briefly, a *hoz* mutant on the cab genetic background was crossed with the HNI strain to obtain the genetically polymorphic F1 offspring. These F1 fish were crossed to obtain the *hoz* mutant embryos for mapping. The pooled bulked segregant analysis was performed to localize the *hoz* mutation on the medaka linkage group (LG) (Postlethwait and Talbot, 1997). Further mapping was done by using custom-designed markers based on the sequence polymorphism between the cab and HNI strains. The following mapping primers and restriction enzymes were used for mapping:

MF01SSA019D03	F: 5′-AAAGGCATCATTACTGGTGT-3′, R: 5′-ACAACTAACTATGGGTCCTG-3′;
ZPC2-3	F: 5′-GCATTCCTTCCTGCCTGACC-3′, R: 5′-AAAGTGGTTACAAGAGGGAGG-3′ (NdeI);
MF01SSA041A11	F: 5′-GTTCAGTGATCCCGTCAATGC-3′, R: 5′-CTATCCGAAGAGTACAGCAGG-3′ (Dde I);
MAP4	F: 5′-CGCTTTTCAGGTCCACCGTTT-3′, R: 5′-CGTCTGGTTCCAACAAGGCTG-3′.

The coding sequence of *vmhc* cDNA was deposited in the GenBank/DDBJ DNA sequence database under an accession number AB515306.

Whole-mount RNA in situ hybridization (ISH) analysis

Whole-mount ISH analysis was performed according to the procedure described previously (Thisse and Thisse, 2008). After staining, tissues were fixed with 4% paraformaldehyde (PFA) in phosphate-buffered saline (PBS) for color preservation, equilibrated with 80% glycerol, and mounted on slide glasses for microscopic observation. The following primers were used for cloning the respective probes:

vmhc F: 5′-GCTGAGATGTCCGTGTATGGTGC-3′, R: 5′-GCTCCTCACGAGGCCTCTGCTTG-3′;
mhc2 F: 5′-TCAGATCACACGGATTATGG-3′, R: 5′-ATGGCAGAGGGGTATCCACC-3′;
amhc F: 5′-TGCACTGATGGCTGAATTTG-3′, R: 5′-ACTTGATCTACACCTTGGCC-3′;
cmlc2 F: 5′-AATGTCTTTTCCATGTTTGAGC-3′; R: 5′-CTCCTCTTTCTCATCCCCATG-3′;
nkx2.5 F: 5′-CCAGCACGTCCACTCCTTTC-3′, R: 5′-TCACCACGTCCTAATGCCG-3′;
bmp10a F: 5′-CATCCGCAGCTTTAAGAACG-3′, R: 5′-TACAGCAGGGAGATGGGGTC-3′;
bmp10b F: 5′-TCATGCTGGAGCTCTACAATCG-3′, R:5′-CGCATTCTGCTACTACCATTCC-3′;
bnp F: 5′-CACAACAGACCGGAACCAGAACC-3′, R: 5′-GGGACGATCTGGACAGTGGG-3′;
jarid2/*jumonji* F: 5′-CCAACACAAATGCATTTACAAGG-3′, R: CGTAGCGAGCAGAAGAGAGC-3′;
tsc2 F: 5′-TACCAGCCGAGCAATGAGG-3′, R: GCCAGGTCCTTGTCTTCAGC-3′;
epo F: 5′-GCTGTTGATTGTGTTGGAGTGG-3′, R: CGCAGGAAGTTCACGTGG-3′;
nrg1 F: 5′-GAATTTACTGGTGATCGCTGCC-3′, R: AAAGCGACTGACGGGACG-3′.

The respective products amplified by the polymerase chain reaction (PCR) were subcloned into standard vectors and used for synthesizing the digoxigenin (dig)-labeled RNA probes.

Electron microscopy and histology

Transmission electron microscopy (TEM) analysis was performed according to the method described earlier (Rottbauer et al., 2001). The paraffin embedding and sectioning were performed according to a standard method using Bouin's fixative. Embedded samples were serially sectioned with a microtome; and the sections were mounted on slide glasses, washed with xylene and ethanol, and stained with hematoxylin and eosin.

Immunohistochemistry

Medaka whole embryos or dissected hearts were fixed by the following procedures. For staining with MF20, an antibody against the myosin heavy chain (Developmental Studies of Hybridoma Bank), embryos were fixed with the IHC Zinc Fixative (BD Biosciences) at room temperature for 20 h. For staining β-catenin (C2206, Sigma), fixation was done with 80% methanol, 20% dimethylsulfoxide (DMSO) at room temperature for 2 h followed by dehydration with methanol at −30 °C. For phalloidin (Invitrogen) staining of F-actin bundles, dissected hearts were fixed with 4% PFA in PBS for overnight at 4 °C. Following fixation and removal of the egg chorion, samples were equilibrated with PBS containing 0.1% Triton X-100 (PBSTx) and further replaced with PBSTx containing 1% DMSO (PBSTxD). Samples were blocked with 2 mg/ml BSA and 5% serum in PBSTxD for 2 h at room temperature and reacted with the above antibodies at 4 °C for overnight. The MF20, anti-β-catenin, and Alexa568-conjugated phalloidin were used at 1:100, 1:1500, and 1:1000 dilutions, respectively. After washing with PBSTxD, the respective secondary antibodies were applied at room temperature for 2 h at 1:1000 dilutions. After washing, samples were mounted in 80% glycerol supplemented with 2.5% 1,4-diazabicyclo [2,2,2] octan (DABCO) as an antifade agent and viewed under a confocal microscope, Fluoview FV1000 (Olympus).

Measurement of ventricle size and the estimation of surface area

The lengths of long (L) and short (S) axes of wild type and *hoz* mutant ventricles at stage 37 were measured from confocal pictures of fixed and dissected hearts. We approximated the ventricle shape as a spheroid, and the surface areas were calculated from the following equation:

$$\text{Surface area} = 2\pi\left\{c^2 + abx E(x,k) + \frac{bc^2}{ax}F(x,k)\right\},$$

$$x = \sqrt{1-\frac{c^2}{a^2}},\ k = \frac{\sqrt{1-\frac{c^2}{b^2}}}{x}.$$

Incomplete elliptic integral of the 1st kind, $F(x,k) = \int_0^x \frac{dt}{\sqrt{(1-t^2)(1-k^2t^2)}}$, $-1 \le x \le 1$.

Incomplete elliptic integral of the 2nd kind, $E(x,k) = \int_0^x \sqrt{\frac{1-k^2t^2}{1-t^2}}\,dt$, $-1 \le x \le 1$.

a, b, and c are the major and minor axes of the spheroid; and in this case, $a = L/2$ and $b = c = S/2$.

BrdU analysis

The cell proliferation analysis was conducted after labeling embryos with BrdU for 20 h starting at stage 34. After incubation in 2 mM BrdU at 28.5 °C, embryos were fixed with 4% PFA for 2 h at room temperature. The fixed embryos were dehydrated with methanol and stored at −20 °C. Immunochemical detection was conducted by the procedure described recently (Yoshinari et al., 2009). The BrdU-labeled fluorescent cells were quantified from the acquired images obtained by a confocal microscopy (Fluoview FV1000, OLYMPUS). We routinely dissected the heart, mounted in an orientation that the ventricle and atrium boundary is clearly visible. More than 100 optical sections were obtained from each heart, and generate the partially stacked images by merging every 20–40 sections. Cell count was carefully performed on these optical slices to exclude the BrdU-labeled cells in non-muscle tissues.

Generation of transgenic fish and cell count

The construct that drives the expression of *DsRed2-nuc* under the control of the zebrafish *cmlc2* promoter was a gift from G. C. Burns (Mably et al., 2003). This construct was injected into fertilized medaka eggs at the 1-cell stage at a dose of 10–40 ng/μl. Embryos with bright fluorescence in the heart were raised, and a stable germ line transmission was established. The resulting transgenic strain was used for scoring the cardiomyocyte numbers in the ventricle. The wild type and *hoz* mutant hearts carrying the *Tg (cmlc: DsRed2-nuc)* were dissected, fixed with 4% PFA in PBS for 10 min at room temperature, and mounted in 1% agarose gel. We routinely made 50–100 optical sections from one heart sample, and cell count was conducted on the merged images of every 25 sections.

2,3-butanedione monoxime (2,3-BDM) treatment

We tested a series of 2,3-BDM concentrations on medaka fish at stage 32. Concentrations higher than 30 μM showed a toxic effect within 24 h; however at concentrations lower than 15 μM, the reagent could not effectively block the heartbeat. For the healthy survival of medaka fish and complete block of heartbeat, we adopted the 2,3-BDM treatment at 22.5 μM for 24 h and 17.5 μM for the following 48 h. Under this condition, the ventricle did not beat, but the atrium showed an occasional and weak beating. In some wild type embryos, the accumulation of blood cells in the atrium was observed, but it did not affect the number of ventricular cardiomyocytes.

RT-PCR analysis

Hearts were harvested from wild type and *hoz* mutant embryos ($n = 40$ for each) at stage 37. Total RNAs were extracted and 5 μg of total RNA was used for cDNA synthesis. The primers for *bnf* and *bmp10* were the same as those used for cloning the *in situ* probes. *ef1α* was amplified with primers: F, 5′-ATCGTTGCTGCTGGTGTTG-3′; R, 5′-AGGCGATGTGAGCTGTGTG-3′, as an internal control. The PCR reaction comprised 94 °C for 30 s, 55 °C for 30 s, and 72 °C for 30 min.

Results

Enlarged ventricle in the medaka hoz mutant

In the previous screening for ENU-induced mutations of medaka fish, we identified several mutants with phenotypes showing abnormal heart development. The *hoz* mutant was a recessive lethal mutant having an abnormally large ventricle. Initial formation of the *hoz* heart tube appeared to be normal until medaka developmental stage 30, a stage that corresponds to the cardiac looping stage (Fig. 1C). However in the subsequent stages of development, their ventricles progressively enlarged (Figs. 1A, B). Despite this abnormality, the mutant survived until 8 dpf, a stage around hatching, in a relatively healthy condition without forming pericardiac edemas.

Observations of the *hoz* ventricle showed that ventricular contraction was inhibited when the ventricle and atrium are segregated at stage 26 (see Supplementary Videos 1 and 2). The blood flow was clogged in the ventricle due to the sustained beating of the atrium, although a very slow stream of blood flow could be seen at stage 37 (data not shown). It is therefore believed that ventricular

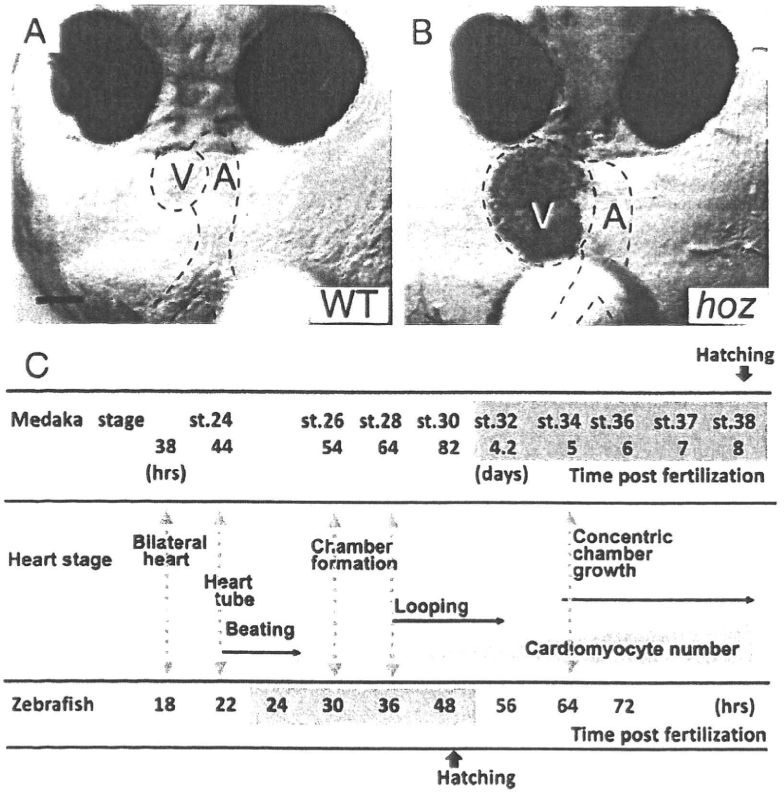

Fig. 1. Ventricle enlargement of the medaka *hoz* mutant. (A, B) Morphology of wild type and *hoz* mutant heart at stage 37. The mutant showed a unique phenotype that the ventricle (V) was extraordinary enlarged and filled with blood cells (panel B), whereas the mutant atrium (A) had a normal appearance (panel A). Due to inability of heart beating in the ventricle (see Videos S1, S2 in the supplementary material), the blood flow was very slow and almost clogged around stage 34. (C) A diagram comparing developmental stages of medaka fish and zebrafish. The medaka developmental stages (top) and the corresponding zebrafish stages are aligned (bottom), in which the key events of heart morphogenesis are indicated in the middle. Though the zebrafish heart mutants with defective beating (Sehnert et al., 2002; Berdougo et al. 2003; Bartman et al., 2004; Auman et al., 2007; Rottbauer et al., 2007) have been mainly analyzed within 48 hpf (highlighted with green), the *hoz* mutant showed a characteristic ventricle enlargement phenotype at the later stage of heart development (highlighted with pink), which was possibly due to its longer survival until 8 dpf in a relatively healthy condition without the formation of pericardiac edemas. The scale bar represents 100 μm in (A).

enlargement was a secondary defect due to heart malfunction. In spite of the defect of blood flow, the overall number of blood cells appeared similar between wild type and mutant embryos during stages 30–39 (data not shown), suggesting that the overall hematopoiesis was not affected in the *hoz* mutant. Furthermore, the beat rate of the *hoz* atrium did not show significant alteration at stage 37 (Table 1), a stage when the enlargement of the *hoz* ventricle became maximum. In comparison to the ventricle, the size of the *hoz* atrium was never affected (Fig. 1B).

Comparing with similar zebrafish heart mutants with defective beating (Sehnert et al., 2002; Berdougo et al. 2003; Bartman et al., 2004; Auman et al., 2007; Rottbauer et al., 2006), which have been mainly analyzed within 48 hpf of zebrafish development (highlighted with green in Fig. 1C), the *hoz* mutant showed a characteristic enlargement of the ventricle at later stages of heart development (highlighted with pink in Fig. 1C). Thus, the *hoz* mutant has a unique later heart phenotype that occurs late in development, likely due to secondary defects caused by the abnormal ventricular contractions.

Loss-of-function mutation in the ventricle myosin heavy chain (mhc1/vmhc) gene in the hoz mutant

To explore the molecular basis of the *hoz* mutant, we determined the responsible gene. Genetic mapping localized the *hoz* locus to medaka linkage group 17, a region located between ZPC2 and MF01SSA041A11 (Fig. 2A). By further fine mapping, we identified a genomic sequence contig of approximately 250 kb length, the entire region of which showed zero recombination with the *hoz* locus (Fig. 2A). The contig contained 4 *myosin heavy chain* (*mhc*) genes, one of which had a strong sequence homology with the *vmhc* gene of zebrafish and other species.

To further narrow down the candidates, we examined the expression of all 5 genes on the contig by in situ RNA hybridization and found that only the *vmhc*-like gene (*mhc1* in Fig. 2A), but not other 4 genes, had an exclusive expression in the ventricle (Fig. 2B), suggesting the *mhc1/vmhc* gene was most likely to be the *hoz* gene. The second gene *mhc2*, which corresponded to the *mMYHC1* gene reported by Ono et al. (2006) (GenBank AB256934), was expressed in the slow skeletal muscle of the somites (data not shown).

Given the unique expression of *mhc1/vmhc* gene in the ventricle, we focused on this gene and performed further analysis. The sequence

Table 1
Heart beating rate of wild type embryos and *hoz* mutant.

	Heartbeat at stage 30	*n*	Heartbeat at stage 37	*n*
Wild type	137 ± 5	7	157 ± 4	4
hoz mutant	136 ± 5	7	152 ± 2	4

Quantitative analysis of heart beating (per minute) at stage 30 and stage 37 at 28.5 °C is shown. Measurement was performed by using the recorded movies. The rate in *hoz* mutant was measured by the atrial beating.

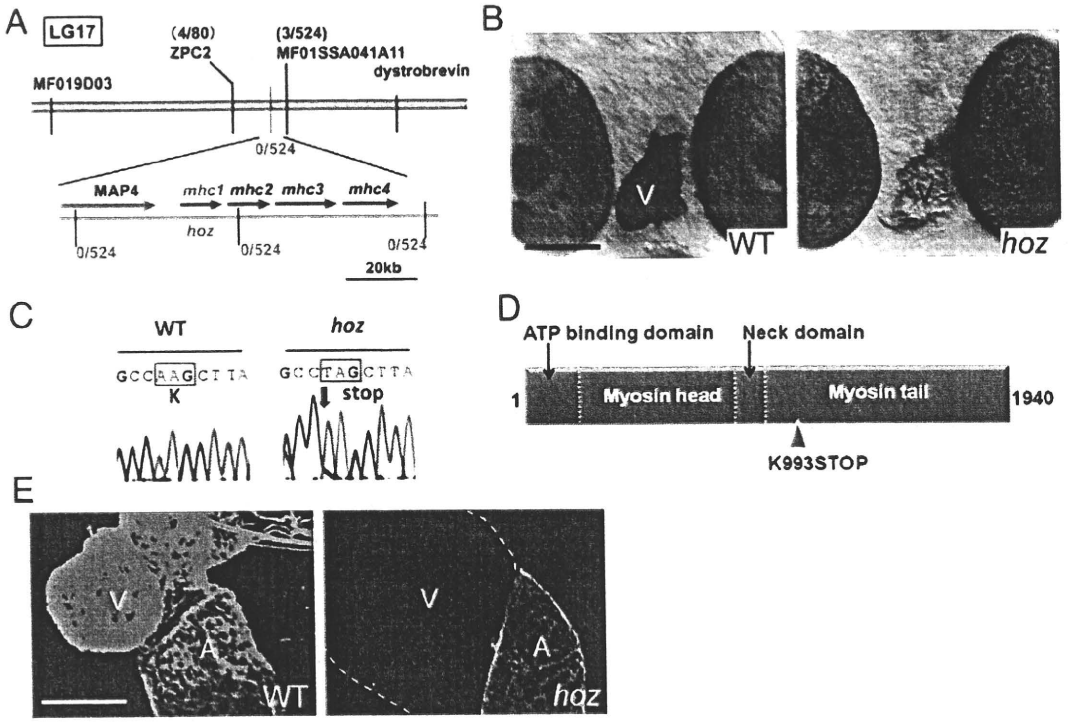

Fig. 2. Identification of *hoz* mutation in the *vmhc* gene. (A) Genetic mapping of *hoz* locus on the medaka linkage group 17. The *hoz* region was located between the ZPC2 (GenBank AF331672) and MF01SSA041A11 (GenBank BJ002936) (upper). Further fine mapping narrowed down the *hoz* locus within a genomic DNA contig with ~250 kb length, which containing 4 copies of myosin heavy chain genes were clustered (lower). No recombination was detected in the entire region of the contig. (B) in situ hybridization analysis detecting *mhc1/vmhc* RNA in the wild type and *hoz* mutant ventricle at stage 30. The *mhc1/vmhc* mRNA was down-regulated in the *hoz* mutant. (C) A nonsense mutation identified in the *mhc1/vmhc* gene, which changed the lysine residue at position 993 to a stop codon. (D) Structure of the ventricle myosin heavy chain (Vmhc) protein and the position of the nonsense mutation in the *hoz* mutant. (E) Absence of Myosin heavy chain (Mhc) protein in the mutant ventricle at stage 34 as revealed by staining with MF20, a pan-Mhc antibody. Staining was seen in the ventricle and atrium of wild type embryos (WT), but absent in the ventricle of the *hoz* mutant (*hoz*). The scale bar represents 100 μm in (B) and (E).

analysis revealed that the *vmhc* gene had a nonsense mutation at the middle of its protein-coding region (Fig. 2C), resulting in the loss of most of the myosin tail domain, which is necessary for the assembly of myosin heavy chains to form their coiled-coil structure (Fig. 2D). Intriguingly, we found that the expression of *mhc1/vmhc* was severely down-regulated in the *hoz* mutant (Fig. 2B), possibly due to the mechanism known as nonsense-mediated RNA decay. We also confirmed that the *hoz* ventricle did not contain the Mhc proteins by staining with the pan-myosin heavy chain antibody, MF20 (Fig. 2E), supporting that there was no compensatory expression of other myosin heavy chains in the ventricle and that the identified mutation in the *mhc1/vmhc* is the cause of loss of ventricle beating. Although we could neither succeed in producing the phenocopy by the morpholino antisense oligonucleotide (MO) nor rescue the *hoz* phenotype with mRNA injection due to the late *hoz* phonotype (3–4 dpf), from these supporting evidences, we concluded that the *hoz* mutation resulted in the complete loss of myosin heavy chain function in the ventricle.

Effect of vmhc mutation on cardiomyocyte differentiation and maturation

We next examined how the heart formation and maturation is affected by the loss of Vmhc function and heart contraction. We evaluated the cardiomyocyte differentiation in the *hoz* mutant by looking at the expression of genes such as *nkx2.5*, *tbx5*, and *mef2c* (Olson, 2006), transcription factors whose products are required for heart development and cardiomyocyte differentiation. However, no significant alteration of their gene expression was observed in the *hoz* heart primordium (Supplementary Figs. 1A–C), suggesting that the heart-field formation and cardiomyocyte differentiation occurred normally in the *hoz* mutant. As well as the regulatory transcription factors, the expression of *cmlc2* and *amhc*, genes encoding the myofibril proteins in the entire heart and atrium, respectively, were neither affected in the *hoz* mutant (Supplementary Figs. 1D, E).

Given the normal differentiation of ventricular cardiomyocytes, we next asked whether or not they matured normally as cardiac muscle cells. To examine the maturation status of ventricular myocytes, we examined their subcellular structures by electron microscopy analysis. In contrast to the thick myofibrils seen in the wild type ventricular cells (see arrow in Fig. 3A), the *hoz* ventricular cells lacked the myofibrils and contractile apparatus (Fig. 3B). However, despite the lack of myofibrils, the mutant ventricular cells retained a number of mitochondria as in the wild type cardiomyocytes (Figs. 3A, B; arrowheads) and stored a number of dense glycogen particles in their cytoplasm (Fig. 3B), suggesting that the cardiomyocyte maturation process somehow occurred in the *hoz* ventricle. On the other hand, we did not see any abnormalities in the atrial myocytes (data not shown).

Defective chamber morphogenesis in the hoz ventricle

A previous study by Auman et al. (2007) on zebrafish mutants with altered *amhc* and *vmhc* genes suggested that cardiac contractility and blood flow are required for proper cell-shape changes and the formation of chamber curvature during heart morphogenesis. In the *hoz* mutant, we visualized the cell shape by staining with anti-β-catenin antibody (Supplementary Figs. 2A–D) and observed that the ventricular cardiomyocyte in the *hoz* mutant is also expanded within the planar dimension and have irregular but hexagonal shapes as in the zebrafish *vmhc* mutant (Auman et al., 2007; Supplementary Fig. 2D). In addition, the phalloidin staining showed that the

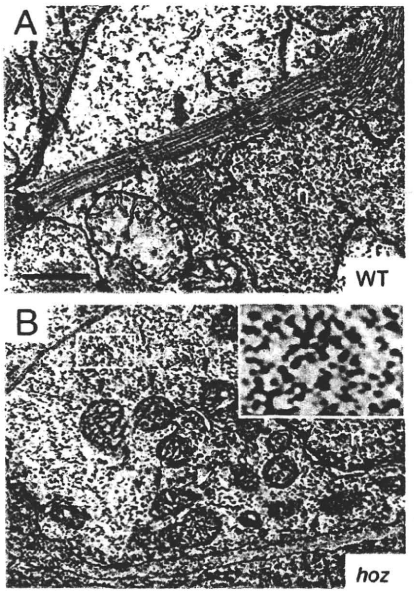

Fig. 3. Normal differentiation and maturation of *hoz* ventricular cardiomyocytes. (A, B) Examination of subcellular structure of wild type (A) and mutant (B) ventricular cells at stage 37 by transmission electron microscopy. Thick myofiber bundles were seen in the cardiomyocytes of the wild type embryo (arrow), but not in those of the *hoz* mutant. Arrowheads indicate the well-developed mitochondria, a hallmark of mature cardiac muscles. Both in wild type and mutant, many glycogen granules, which are also a sign of mature cardiomyocytes, were present within the ventricular cardiomyocytes. A high-magnification view of glycogen granules (boxed area in B) is shown in the upper right corner. The observations were confirmed by examining more than 90 sections through the heart region from each of 3 wild type and 2 mutant embryos. n, nucleus. The scale bar represents 1 μm in (A).

formation of contractile F-actin cables, which are associated with myosin heavy chains, was missing in the *hoz* mutant (Supplementary Figs. 2E, F), indicating that the loss of myosin heavy chain affects the formation of F-actin bundles.

In addition to such a phenotype in the cardiomyocyte cell shape, we found that the concentric chamber growth was also impaired. Following the stage of cardiac looping and the formation of curvature, the cardiac chambers increase thickness of the wall through the concentric growth, and give rise to the trabeculated chambers in the adult animal. The concentric growth of the ventricular wall begins in medaka fish at stage 34, when the wall thickness is 1–2 cell layers (Fig. 4A). By stage 36, 3–4 layers of cardiomyocytes can be recognized (Fig. 4C). In the *hoz* mutant, the ventricular wall was also 1–2 layers at stage 34 and remained so at stage 36 (Figs. 4B, D), even after stage 37. To further confirm this phenotype, we utilized the *Tg (cmlc2:DsRed2-nuc)* embryo, in which the identity of cardiomyocytes was visible by the expression of DsRed2 in the nucleus, and revealed that the lack of cardiomyocyte layers indeed occurred in the *hoz* mutant (Figs. 4E, F). Thus, the loss of Vmhc function affected the concentric chamber growth in the later phase of heart development.

Excess production of cardiomyocytes in the hoz ventricle

As we have shown in Fig. 1B, the *hoz* ventricle was strikingly enlarged. We suspected that merely the cell-surface expansion and lack of concentric growth could not account for it. Indeed, according to our estimation (Fig. 5A), the surface area of the *hoz* ventricle was approximately 6 times greater than that of the wild type one at stage 37 (Fig. 5B). Taking the decrease of concentric growth in account, which increases the surface area by 2 times, there was still a 3-fold increase in the surface area. Judging from the spacing of cardiomyocyte nuclei (Figs. 4E, F), the expansion of each cell surface may not be as big as 3 times. Therefore, we suspected that an increase in cell number might have been responsible for the ventricular enlargement.

We examined cell proliferation by labeling with BrdU during stages 34–36 (Fig. 5C). Though it has been suggested that the cardiomyocyte proliferation rate is relatively low before the heart looping stage in chick and zebrafish (Soufan et al., 2006; de Pater et al., 2009), the rate after the looping stage (Fig. 1C) appeared to be higher, possibly due to the rapid increase of the thickness of chamber wall. We indeed observed that a number of BrdU-labeled cells were present in the entire chamber wall region of the wild type heart by examining the confocal optical sections. Using the confocal images, we carefully counted the BrdU-labeled cells within the cardiomyocyte layers and revealed a detectable increase of the number of BrdU-positive cells (~1.4 fold) in the *hoz* ventricle (Fig. 5D), although the statistical significance was not sufficient ($P<0.1$), which was probably due to the higher number of proliferating cardiomyocytes in this stage and inevitable count of the endocardium and blood cells.

To precisely determine the number of cardiomyocyte, we used the *Tg (cmlc2:DsRed2-nuc)*, expressing DsRed in the cardiomyocyte nuclei (Figs. 5E, F). As in the BrdU analysis, we quantified the number of cardiomyocytes by using confocal images and found that the *hoz* mutant ventricle displayed a significant increase in the number of cardiomyocytes compared with the wild type ventricle at stage 34 and stage 37; whereas the difference was not evident at stage 30 (Fig. 5F). Such increase was more evident at stage 37 (wild type: 261 ± 20; *hoz* mutant: 413 ± 16). Therefore, the number of cardiomyocytes in the *hoz* ventricle increased more than 1.5 times than that of the wild type one. Since the number of cardiomyocytes in wild type embryos was 332 ± 20 ($n=4$) even at stage 39, 2 days after stage 37, we concluded that an excess number of cardiomyocytes were added in the *hoz* ventricle during later phase of heart development. In contrast to the increase of ventricular cardiomyocyte, we did not see any detectable alterations in cardiomyocyte number, shape and size in the atrium, although we did not perform an accurate quantification.

Induction of bnp and bmp10 family gene expression in the hoz ventricle in response to the increased cardiac pressure

Progressive enlargement of the ventricle often accompanies elevated cardiac pressure. We therefore investigated whether the loss of ventricular beating caused a stress on the developing ventricle. To evaluate the stressed status of ventricle, we looked at the expression of *natriuretic peptide* genes. As a modulator of cardiac function, this family of proteins, which is induced in the hypertrophic and dilated cardiomyopathies of mammals, is known to be the most powerful neurohumoral predictor of left-ventricular function and prognosis (Cameron and Ellmers, 2003; Clerk et al., 2007). Though the *atrial natriuretic peptide* (*anp*) gene is widely used as a marker for cardiac stress, medaka fish does not have an exact ortholog (Inoue et al., 2003; our database search). Instead, we used the *brain natriuretic peptide* (*bnp*) gene, which is also known to have similar functions and to be induced by physiological stresses (Tokola et al., 2001; Cameron and Ellmers, 2003). The results of in situ expression and RT-PCR analysis showed that the expression of *bnp* was strongly elevated only in the ventricle (Figs. 5G, H), confirming that the *hoz* ventricle was exposed to a stressed status.

We next examined the expression of molecules such as *tsc2* (Pasumarthi et al., 2000), *epo* (Stuckmann et al., 2003), *nrg1* (Ford et al., 1999), *jarid2/jumonji* (Toyoda et al., 2003), *fgf2* (Sheikh et al., 1999), *raldh2* (Keegan et al., 2005; Wills et al., 2008), and *bmp10* (Chen et al., 2004) that are implicated in the regulation of heart growth. Among them, only the expression of the *bmp10a* and *bmp10b* genes exhibited apparent up-regulation in the *hoz* ventricle (Figs. 5G, H), while *bmp10a* showed a weaker expression (data not shown).

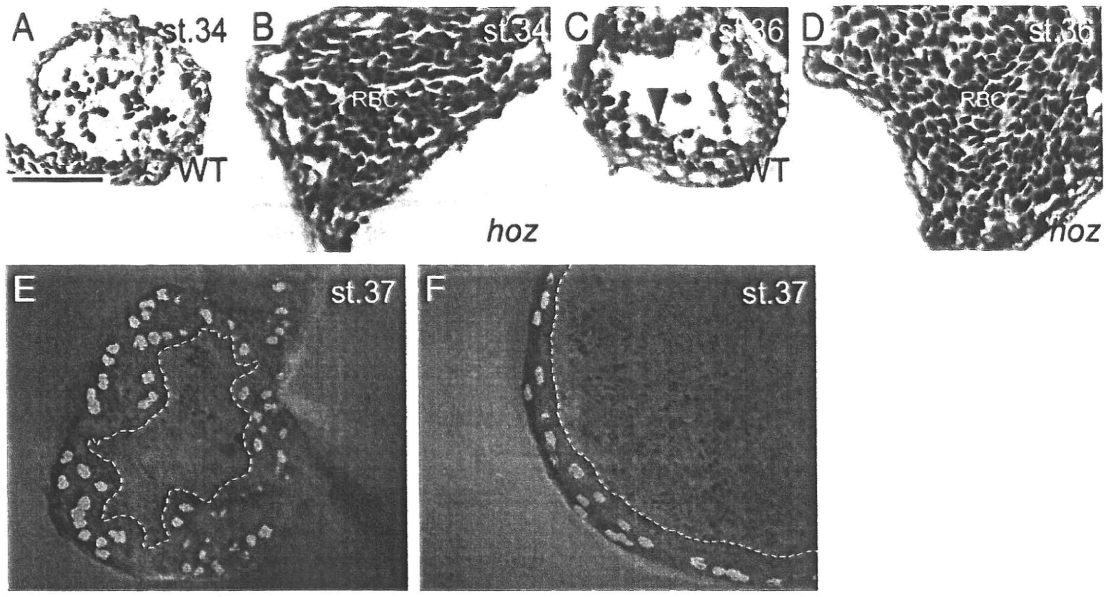

Fig. 4. Impaired concentric layer growth of ventricular chamber in the *hoz* mutant. (A–D) Histological analysis of the ventricular wall in wild type (A, C) and *hoz* (B, D) ventricles at stage 34 (A, B) and stage 36 (C, D). Paraffin sections were counter-stained with hematoxylin and eosin. The *hoz* ventricle was filled with blood cells, most of which were nucleated red blood cells (RBC). The concentric growth of the ventricular wall was not evident at stage 34 (A, B). But at stage 36, 3–4 cells layers were apparently observed (C), whereas the ventricular wall of the *hoz* mutant remained 1–2 layers at this stage (D). (E, F) Confocal optical sections of ventricular chambers of wild type (E) and *hoz* mutant (F) at stage 37, in which the cardiomyocytes were visualized by the *Tg (cmlc2:DsRed2-nuc)*. The defect in concentric growth of cardiomyocyte layers is clearly observed in the *hoz* ventricle. The scale bar represents 50 μm in (A). All pictures are at the same magnification.

Regulation of cardiomyocyte production and bmp10b induction by elevated cardiac pressure

It has been proposed that intracardiac hemodynamics and blood pressure act as a key epigenetic factor in embryonic cardiogenesis (Hove et al., 2003). Therefore, we next examined whether or not the increase in cardiomyocyte number in the *hoz* mutant depended on the elevated cardiac pressure caused by the inability of ventricular beating. In order to dissect the effect of cardiac pressure, the morpholino antisense oligonucleotide against *troponin T* was successfully used to abolish the heartbeat in zebrafish (Sehnert et al., 2002); however it could not be applied to reduce the heart beating in medaka fish due to the long developmental period. In this study, we firstly adopted an approach to manipulate the blood flow without affecting myocardial function. In contrast to the zebrafish, the veins in medaka fish that flow into the sinus venosus (SV) are arranged into 3 major ducts, i.e., the 2 common cardinal veins (CCV) located laterally and the marginal vein (MV) from the caudal region (Fig. 6A; Fujita et al., 2006). By firmly pinching and crushing these veins with forceps at stage 32, we succeeded in blocking the blood flow (Figs. 6B, C).

Such an operation could reduced the blood inflow into the atrium; and the fluid between the ventricle and operated sites moved back and forth, resulting in the alleviation of excess blood pressure in the *hoz* mutant. In the *hoz* embryos in which blood flow was not present at stage 37 (3 of 7 operated embryos), the average number of cardiomyocytes (239 cells; Fig. 6E) was comparable with that of operated wild type (255 cells, $n=2$) (Fig. 6D) and un-operated wild type embryos (see Figs. 5E, F). Moreover, embryos in which flow was partially blocked showed an intermediate phenotype (327 cells, $n=3$). These data supports that the cardiomyocyte increase observed in the *hoz* mutant ventricle depended on the elevated cardiac pressure.

Because the mechanical blockade was not a perfectly successful method due to occasional recovery of crashed blood vessel, we further performed a pharmacological blockade of blood flow. In zebrafish, reagents such as 2,3-butanedione monoxime (2,3-BDM), which blocks myofibrillar ATPase, was used to reduce the heartbeat (Bartman et al., 2004; Auman et al., 2007). In medaka embryo, the reagent affected the heartbeat at higher concentrations than that for zebrafish. At the condition we used, the ventricle was completely silent, but the atrium occasionally beat at a very slow rate in some embryos. Under this condition, almost all embryos survived in a healthy condition up to 3 days from stage 32 to 37 (Figs. 6F, G). In the *hoz* embryos treated with 2,3-BDM, the morphology of the ventricle was apparently smaller than the untreated *hoz* ventricle and similar to that of wild type (Figs. 6F, G). The number of cardiomyocytes was comparable with that of wild type embryos treated with the reagent (Figs. 6H–J). Intriguingly, the lack of concentric growth in the *hoz* ventricle was also rescued by the decreased cardiac pressure (Figs. 6E, I), suggesting

Fig. 5. Aberrant increase in number of cardiomyocytes in the *hoz* ventricle. (A) Measurement of the ventricle size. The surface areas of wild type (WT) and *hoz* mutant ventricles were estimated from the average lengths of the long (*L*) and short axes (*S*). BA, bulbus arteriosus; V, ventricle; A, atrium. (B) Increase in ventricular surface area in *hoz* mutant. Calculation was performed based on the measurement of long and short axes of ventricle (A) according to the equation described in the Methods section. Data are presented as the mean ± SEM. Statistical significance was tested by using Student's *t*-test. $^{*}P<0.01$. (C) Confocal stacked images of wild type and *hoz* mutant hearts, in which the labeled BrdU during stage 34–35 was detected by the anti-BrdU antibody staining. (D) Quantification of BrdU-labeled cells. Cell count was performed on the confocal images to exclude the labeling in non-muscle regions such as the blood cells and endocardial cells. Data are presented as the mean ± SEM. Statistical significance was tested by the use of Student's *t*-test. $^{*}P<0.1$ ($n=11$ for wt, $n=9$ for *hoz*). (E) Confocal stacked images of wild type and *hoz* mutant hearts that harbor the *Tg (cmlc2:DsRed2-nuc)* at stage 37. These pictures are reconstructed confocal images, in which approximately half of the cardiomyocytes are visible. (F) Quantification of ventricular cardiomyocytes using the transgenic line. Cell counting was performed on the confocal images. Data are presented as the mean ± SEM. Statistical significance was tested by using Student's *t*-test. NS, statistically not significant at $P=0.01$ ($n=5$ for WT and *hoz*, respectively). $^{*}P<0.01$ ($n=5$ for WT and *hoz*, respectively, at stage 34; $n=7$ for WT and $n=6$ for *hoz* at stage 38). (G, H) Induction of *bnp* and *bmp10b* expression in response to the elevated cardiac pressure. In situ RNA hybridization analysis (G) detected the strong expression of *brain natriuretic peptide (bnp)* at stage 37 and *bmp10b* at stage 34 in the mutant ventricle (V), whereas only a faint expression was detected in wild type. RT-PCR analysis of the expression levels of *bnp*, *bmp10b*, *ef1α*, and *amhc*, in wild type (W) and *hoz* mutant (M) embryos at stage 37 (H) quantitatively supported the induction of *bnp* and *bmp10b* in the *hoz* heart. The number of PCR amplification cycle were 28 cycles for *amhc* and *bnp*, 27 cycles for *bmp10b*, and 23 cycles for *ef1α*. V, ventricle; A, atrium. The scale bar represents 50 μm in (C) and (E), and 100 μm in (G).

that the ability for concentric growth is retained in the *hoz* ventricle and that the increased cardiac pressure impairs the proper chamber growth.

In spite of the rescue of *hoz* phenotypes, the 2,3-BDM treatment significantly reduced the cardiomyocyte proliferation in the wild type embryos (Fig. 6J). This raises possibilities that the cardiac pressure is a necessary driving force to support the cardiomyocyte proliferation or that 2,3-BDM affected the cell proliferation by a side effect that is independent of the cardiac pressure. Considering the result of blood vessel operation and the healthy heart development including the concentric chamber growth in the presence of 2,3-BDM, the former possibility seems to be more plausible than the side effect of 2,3-BDM.

To further examine the causal relation between the cardiac pressure, cardiomyocyte increase, and the induction of *bmp10*, we looked at the expression of *bmp10b* in the embryos in which the cardiac pressure was lowered by the 2,3-BDM treatment (Figs. 6K, L). The *bmp10b* expression was apparently reduced in embryos treated with 2,3-BDM (Fig. 6L; $n=8$). The data supports that the *bmp10*

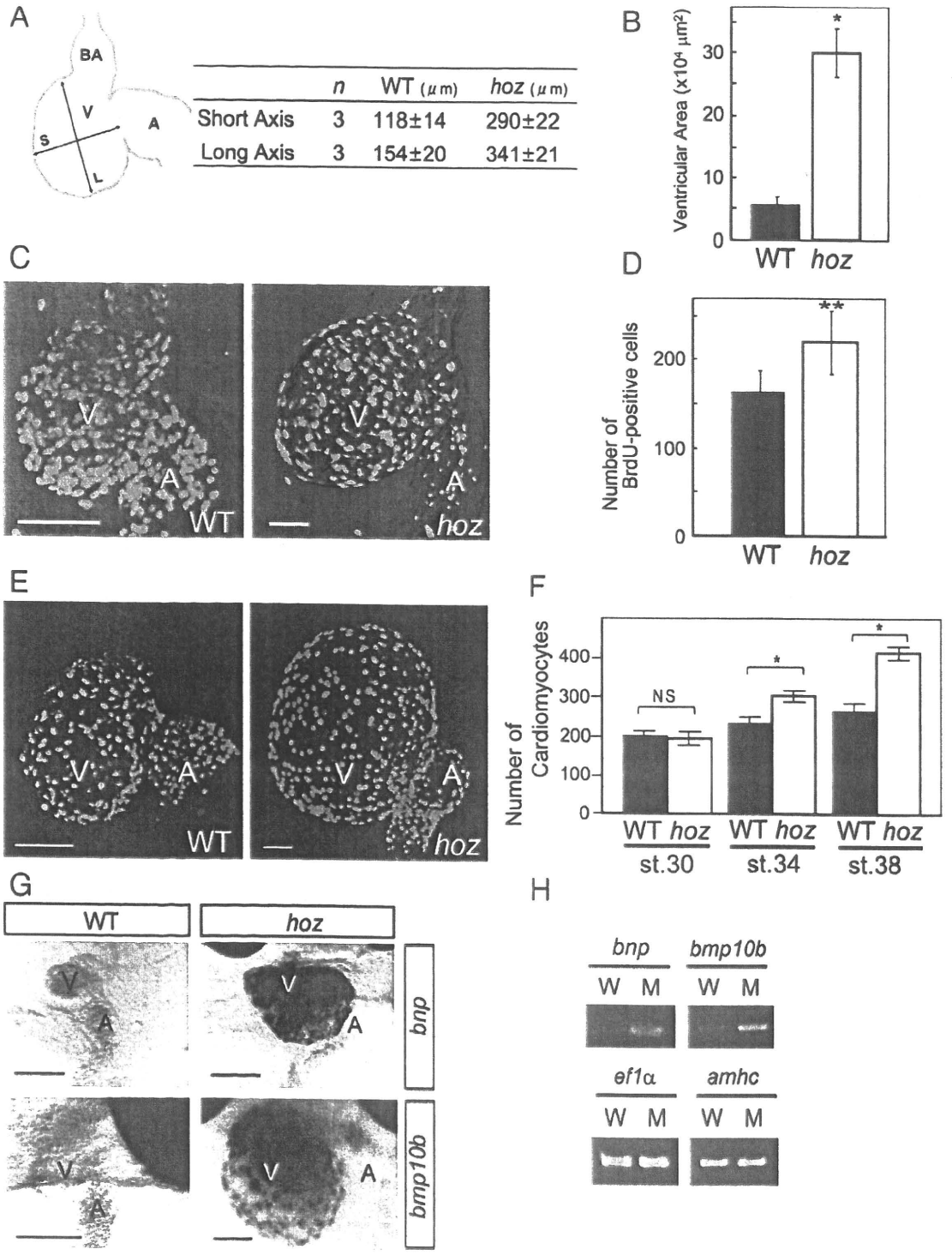

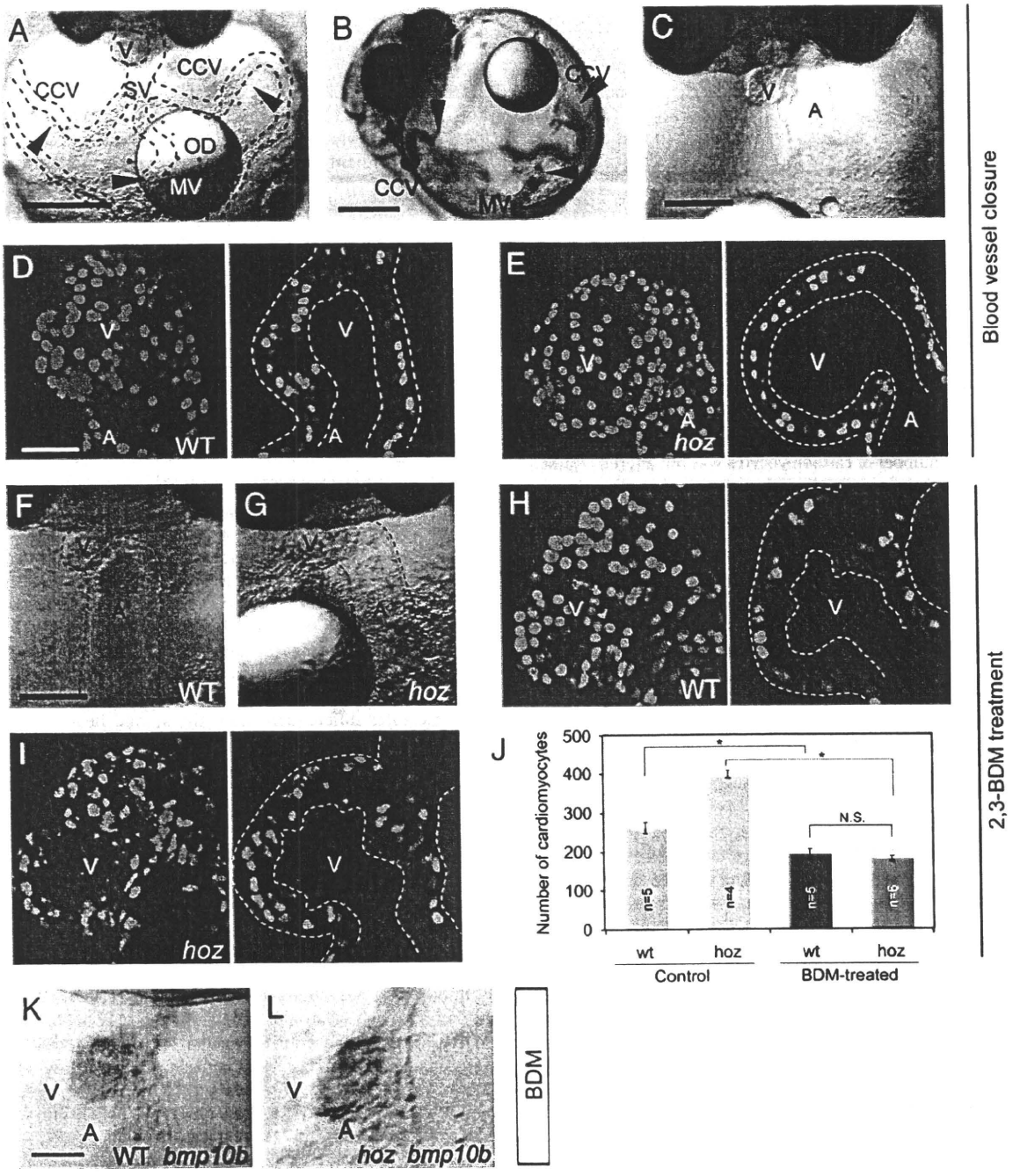

Fig. 6. Influence of elevated cardiac pressure on cardiomyocyte proliferation. (A–C) Outline of the blood vessel blockage experiment. In medaka embryo at stage 32, the venous blood inflows into the sinus venosus (SV) through 3 major veins, i.e., the 2 common cardinal veins (CCV) and the marginal vein (MV), which run on the surface of the yolk (A) (Fujita et al., 2006). By mechanically crushing these veins (arrowheads in A and B), the blood flow into the heart was blocked (C). (D, E) Visualization of cardiomyocytes in the operated embryos. Cardiomyocytes of wild type (D) and *hoz* mutant (E) embryos at stage 37 were visualized by the *Tg (cmlc2:DsRed2-nuc)*. These pictures were reconstructed from confocal images, and only approximately half of the cardiomyocytes are visible. Respective right-side panels show the confocal optical sections through the center of the ventricle. (F, G) Appearance of wild type (F) and *hoz* (G) hearts treated with the 2,3-BDM. (H, I) Cardiomyocytes in the BDM-treated wild type (H) and *hoz* (I) embryos at stage 37. These pictures were reconstructed from confocal images, and the respective right-side panels show the confocal optical sections. (J) Quantification of the number of cardiomyocytes in embryos treated with the 2,3-BDM. Data are presented as the mean ± SEM. Statistical significance was tested by use of Student's *t*-test. **P* 0.01. N.S., not significant. (K, L) Down-regulation of *bmp10b* in the *hoz* embryos treated with 2,3-BDM. The induction of *bmp10b* in the *hoz* embryos was suppressed ($n = 8$; compare with Fig. 5G). The 2,3-BDM treatment did not induce the *bmp10b* expression in wild type embryos ($n = 5$). OD, oil droplet; V, ventricle; A, atrium. The scale bar represents 200 μm in (A) and (B), 100 μm in (C), (F) and (K), and 50 μm in (D). The images in (D, E, H, I) are at the same magnification.

expression is under the regulation of the elevated cardiac pressure. Taken together, our results suggest that Bmp10, which has been suggested to promote the cardiomyocyte proliferation in mammals, may act as a mediator for the cardiomyocyte increase in the *hoz* mutant in response to the elevated cardiac pressure.

Discussion

The heart begins to function long before its formation is complete. It is known that cardiomyocytes are produced almost exclusively during development, and hence it has been thought that the number

of cardiomyocytes is simply determined according to the genetic program. In this study, by analyzing the medaka *vmhc* mutant, *hoz*, we demonstrated that the cardiomyocyte number is influenced by elevated cardiac pressure presumably through the induction of Bmp10, a potent mitogenic factor for cardiomyocytes. Our results suggest the presence of a compensatory mechanism that modulates the production of cardiomyocyte in response to an altered physiological condition, which could also be at play in response to stressed conditions even in postnatal stages.

Later occurring increase of cardiomyocyte number in the hoz mutant

The analysis of zebrafish mutations has suggested a relationship of cardiomyocyte dysfunction and resulting hemodynamic stress and/or elevated cardiac pressure with heart morphogenesis (Sehnert et al., 2002; Xu et al., 2002; Berdougo et al., 2003; Rottbauer et al., 2006; Auman et al., 2007). Though these mutations cause heart dilation, the number of cardiomyocytes has not been extensively addressed. Only for the *haf* mutant, in which the *vmhc* gene is disrupted, it has been reported that the number of cardiomyocytes was not altered (Auman et al., 2007), which is in contrast with our analysis of the medaka *vmhc* mutant, *hoz*. The reason for this difference may be due to the stages analyzed. In zebrafish, the heart looping is completed at 2 days post fertilization (dpf), whereas the looping occurs at 3 dpf in medaka fish among the 8–9 days of embryonic development (Fig. 1C). Though the number of cardiomyocytes in the *haf* mutant was counted at 2 dpf (Auman et al., 2007), we did not see any difference between wild type and *hoz* embryos at the corresponding medaka stage 30 (Fig. 5F). The difference became apparent only in the successive stages. Furthermore, as the *hoz* mutant can survive more than 5 days after stage 30, the slow development and longer progression of the phenotype could make the phenotype clear in medaka fish.

Cell-surface extension and cell-shape abnormality in the hoz mutant

On the other hand, a similar phenotype to the zebrafish *haf* mutant was also observed in cell-shape and surface-area extension (Supplementary Fig. 2D). Though we did not analyze the detail of this phenotype, it seemed that the surface area was slightly extended in the mutant cardiomyocytes. Considering the 1.6-fold increase in cardiomyocyte proliferation and 2-fold increase of the number of surface cells due to the lack of concentric growth, the surface-area extension of each cardiomyocyte would be expected to be 1.75-fold in the *hoz* mutant for attaining the 5.6-fold increase in the total ventricular surface area. This calculation corresponds to the measured cell-surface extension, 1.8-times, found in the zebrafish *haf* mutant (Auman et al., 2007), suggesting that a similar extent of cell-surface extension occurs in the *hoz* mutant.

Concentric growth of cardiac chambers

Another phenotype that we found in the medaka *hoz* mutant was the lack of concentric chamber growth of the ventricle. It has been suggested that a signal emanating from the endocardium regulates the concentric chamber growth (Mably et al., 2006). Within cardiomyocytes, the cardiomyocyte cell polarity such as the oriented formation of myofibers plays an important role in heart morphogenesis and concentric chamber growth (Sultana et al., 2008). Moreover, an intrinsic signaling mechanism that associates with the contractile machinery and/or signaling scaffold such as the Titin complex might also be involved in the concentric growth of chamber (Granzier and Labeit, 2005; Linke, 2008). Therefore, a proper heartbeat, sarcomere function and/or orientation could be required for mediating the signal to direct the dimension of chamber growth.

However, our experiments blocking the blood flow suggested that the *hoz* ventricle retains the ability for the concentric growth and that it can perform a considerable extent of concentric growth when the cardiac pressure was decreased. This suggests that the concentric growth can occur in the absence of the myofiber and heart beating. Possibly, the concentric growth in the *hoz* mutant may be suppressed by the improper cell polarity caused by a strong mechanical overload toward the planar direction and/or the shortage of cardiomyocyte supply to sufficiently support the increase of chamber growth.

Another interesting phenotype of *hoz* mutant was that the lack of contractile apparatus and inability of ventricular beating did not affect the cardiomyocyte maturation itself, suggesting that the cardiomyocyte maturation is independent from the heart beating and elevated cardiac pressure. The cardiomyocyte maturation as a muscle cell might be regulated by other factors such as the Nkx2.5, Tbx5, and Mef2c, which control cell differentiation. Consistent with this idea, the expression of these genes was not affected in the *hoz* mutant.

Epigenetic regulation of cardiomyocyte number in response to elevated cardiac pressure

An important implication made from our analysis is that cardiomyocyte production during development is determined not only by genetic program, but also by epigenetic conditions. The number of cardiomyocytes increased as much as 1.6-fold by the increased blood pressure. Such a fluctuation in cardiomyocyte number generated during development may affect the heart function throughout the life of an animal (Leu et al., 2001). Thus, we suggested that the cardiomyocyte proliferation in response to epigenetic influences is a major cause of increased cardiomyocytes; however, it has recently been proposed in zebrafish as well as amniotes that cardiomyocytes differentiate from the second heart field (SHF) to support the cardiomyocyte number increases during cardiac looping (de Pater et al., 2009). So, there is a possibility that the number of cell in the ventricle increases by recruitment and differentiation of cells from the SHF. However, our quantification of cell proliferation at stage 34–35 showed 1.4-fold increase of BrdU-positive cardiomyocytes, which is comparable to the actual increase of cardiomyocytes (stage 34, 1.3 fold; stage 38, 1.6-fold) revealed by the *Tg* (*cmlc2:DsRed2-nuc*). In addition, the ventricle enlargement in the *hoz* becomes apparent after the heart looping. Therefore, it is likely that the observed cardiomyocyte increase in the *hoz* mutant may mainly reflect the cell proliferation within the ventricle.

Importantly, we observed that Bmp10 was induced in the *hoz* ventricle. Though we do not have a direct functional test of medaka Bmp10, the BMP10 function for cardiomyocyte proliferation has been well documented in mammals (Chen et al., 2004; Pashmforoush et al., 2004). More recently, up-regulation of Bmp10 expression in the hypertrophic rat heart has been observed, and its implication in adaptive myocardial hypertrophy has been made (Nakano et al., 2007). From these and other studies in mammals, it is highly probable that Bmp10 has a function in supporting excess cardiomyocyte proliferation of the *hoz* mutant. Other than Bmp10, a number of other proteins such as the Reptin and Pontin (Rottbauer et al., 2002), L-type calcium channel (Rottbauer et al., 2001), and PDGF (Lien et al., 2006) also have functions for controlling cardiomyocyte proliferation. However, since Bmp10 is the only molecule whose expression was induced in the *hoz* mutant, the Bmp10 expression in response to stressed conditions may play a compensatory role that tunes the heart formation. Hence, any mis-regulation of the mechanism during development could lead to congenital heart disorders (Bartman et al., 2004), and it could also affect the cardiomyocyte proliferation (Bergmann et al., 2009) and hypertrophic growth in cardiomyopathies (Akazawa and Komuro, 2003; Oka et al., 2007; Ransom and Srivastava, 2007) even in the postnatal periods.

Considering the function of Bmp10 protein in promoting cardiomyocyte proliferation (Chen et al., 2004), induction of *bmp10* in

response to increased blood pressure may explain the aberrant production of cardiomyocytes in the *hoz* ventricle.

Acknowledgments

We thank G. C. Burns for providing the plasmid of zebrafish *cmlc2: DsRed2-nuc* construct. This work was supported by grants from the Ministry of Education, Culture, Sports, Science and Technology (MEXT) of Japan.

Appendix A. Supplementary data

Supplementary data associated with this article can be found, in the online version, at doi:10.1016/j.ydbio.2010.01.014.

References

Akazawa, H., Komuro, I., 2003. Roles of cardiac transcription factors in cardiac hypertrophy. Circ. Res. 92, 1079–1088.

Auman, H.J., Coleman, H., Riley, H.E., Olale, F., Tsai, H.J., Yelon, D., 2007. Functional modulation of cardiac form through regionally confined cell shape changes. PLoS Biol. 5, e53.

Bartman, T., Walsh, E.C., Wen, K.K., McKane, M., Ren, J., Alexander, J., Rubenstein, P.A., Stainier, D.Y., 2004. Early myocardial function affects endocardial cushion development in zebrafish. PLoS Biol. 2, E129.

Berdougo, E., Coleman, H., Lee, D.H., Stainier, D.Y., Yelon, D., 2003. Mutation of weak atrium/atrial myosin heavy chain disrupts atrial function and influences ventricular morphogenesis in zebrafish. Development 130, 6121–6129.

Bergmann, O., Bhardwaj, R.D., Bernard, S., Zdunek, S., Barnabe-Heider, F., Walsh, S., Zupicich, J., Alkass, K., Buchholz, B.A., Druid, H., Jovinge, S., Frisen, J., 2009. Evidence for cardiomyocyte renewal in humans. Science 324, 98–102.

Beltrami, A.P., Urbanek, K., Kajstura, J., Yan, S.M., Finato, N., Bussani, R., Nadal-Ginard, B., Silvestri, F., Leri, A., Beltrami, C.A., Anversa, P., 2001. Evidence that human cardiac myocytes divide after myocardial infarction. N. Engl. J. Med. 344, 1750–1757.

Cameron, V.A., Ellmers, L.J., 2003. Minireview: natriuretic peptides during development of the fetal heart and circulation. Endocrinology 144, 2191–2194.

Chen, H., Shi, S., Acosta, L., Li, W., Lu, J., Bao, S., Chen, Z., Yang, Z., Schneider, M.D., Chien, K.R., Conway, S.J., Yoder, M.C., Haneline, L.S., Franco, D., Shou, W., 2004. BMP10 is essential for maintaining cardiac growth during murine cardiogenesis. Development 131, 2219–2231.

Clerk, A., Cullingford, T.E., Fuller, S.J., Giraldo, A., Markou, T., Pikkarainen, S., Sugden, P.H., 2007. Signaling pathways mediating cardiac myocyte gene expression in physiological and stress responses. J. Cell Physiol. 212, 311–322.

de Pater, E., Clijsters, L., Marques, S.R., Lin, Y.F., Garavito-Aguilar, Z.V., Yelon, D., Bakkers, J., 2009. Distinct phases of cardiomyocyte differentiation regulate growth of the zebrafish heart. Development 136, 1633–1641.

Gassmann, M., Casagranda, F., Orioli, D., Simon, H., Lai, C., Klein, R., Lemke, G., 1995. Aberrant neural and cardiac development in mice lacking the ErbB4 neuregulin receptor. Nature 378, 390–394.

Ford, B.D., Loeb, J.A., Fischbach, G.D., 1999. Neuregulin stimulates DNA synthesis in embryonic chick heart cells. Dev. Biol. 214, 139–150.

Fujita, M., Isogai, S., Kudo, A., 2006. Vascular anatomy of the developing medaka, *Oryzias latipes*: a complementary fish model for cardiovascular research on vertebrates. Dev. Dyn. 235, 734–746.

Granzier, H.L., Labeit, S., 2005. Titin and its associated proteins: the third myofilament system of the sarcomere. Adv. Protein Chem. 71, 89–119.

Hove, J.R., Koster, R.W., Forouhar, A.S., Acevedo-Bolton, G., Fraser, S.E., Gharib, M., 2003. Intracardiac fluid forces are an essential epigenetic factor for embryonic cardiogenesis. Nature 421, 172–177.

Inoue, K., Naruse, K., Yamagami, S., Mitani, H., Suzuki, N., Takei, Y., 2003. Four functionally distinct C-type natriuretic peptides found in fish reveal evolutionary history of the natriuretic peptide system. Proc. Natl. Acad. Sci. U. S. A. 100, 10079–10084.

Iwamatsu, T., 2004. Stages of normal development in the medaka *Oryzias latipes*. Mech. Dev. 121, 605–618.

Keegan, B.R., Feldman, J.L., Begemann, G., Ingham, P.W., Yelon, D., 2005. Retinoic acid signaling restricts the cardiac progenitor pool. Science 307, 247–249.

Kimura, T., Yoshida, K., Shimada, A., Jindo, T., Sakaizumi, M., Mitani, H., Naruse, K., Takeda, H., Inoko, H., Tamiya, G., Shinya, M., 2005. Genetic linkage map of medaka with polymerase chain reaction length polymorphisms. Gene 363, 24–31.

Lavine, K.J., Yu, K., White, A.C., Zhang, X., Smith, C., Partanen, J., Ornitz, D.M., 2005. Endocardial and epicardial derived FGF signals regulate myocardial proliferation and differentiation in vivo. Dev. Cell 8, 85–95.

Lee, K.F., Simon, H., Chen, H., Bates, B., Hung, M.C., Hauser, C., 1995. Requirement for neuregulin receptor erbB2 in neural and cardiac development. Nature 378, 394–398.

Leu, M., Ehler, E., Perriard, J.C., 2001. Characterisation of postnatal growth of the murine heart. Anat. Embryol. (Berl.) 204, 217–224.

Lien, C.L., Schebesta, M., Makino, S., Weber, G.J., Keating, M.T., 2006. Gene expression analysis of zebrafish heart regeneration. PLoS Biol. 4, e260.

Linke, W.A., 2008. Sense and stretchability: the role of titin and titin-associated proteins in myocardial stress-sensing and mechanical dysfunction. Cardiovasc. Res. 77, 637–648.

Mably, J.D., Mohideen, M.A., Burns, C.G., Chen, J.N., Fishman, M.C., 2003. heart of glass regulates the concentric growth of the heart in zebrafish. Curr. Biol. 13, 2138–2147.

Mably, J.D., Chuang, L.P., Serluca, F.C., Mohideen, M.A., Chen, J.N., Fishman, M.C., 2006. santa and valentine pattern concentric growth of cardiac myocardium in the zebrafish. Development 133, 3139–3146.

Meyer, D., Birchmeier, C., 1995. Multiple essential functions of neuregulin in development. Nature 378, 386–390.

Nakano, N., Hori, H., Abe, M., Shibata, H., Arimura, T., Sasaoka, T., Sawabe, M., Chida, K., Arai, T., Nakahara, K., Kubo, T., Sugimoto, K., Katsuya, T., Ogihara, T., Doi, Y., Izumi, T., Kimura, A., 2007. Interaction of BMP10 with Tcap may modulate the course of hypertensive cardiac hypertrophy. Am. J. Physiol. Heart Circ. Physiol. 293, H3396–3403.

Oka, T., Xu, J., Molkentin, J.D., 2007. Re-employment of developmental transcription factors in adult heart disease. Semin. Cell Dev. Biol. 18, 117–131.

Ono, Y., Liang, C., Ikeda, D., Watabe, S., 2006. cDNA cloning of myosin heavy chain genes from medaka *Oryzias latipes* embryos and larvae and their expression patterns during development. Dev. Dyn. 235, 3092–3101.

Olson, E.N., 2006. Gene regulatory networks in the evolution and development of the heart. Science 313, 1922–1927.

Pashmforoush, M., Lu, J.T., Chen, H., Amand, T.S., Kondo, R., Pradervand, S., Evans, S.M., Clark, B., Feramisco, J.R., Giles, W., Ho, S.Y., Benson, D.W., Silberbach, M., Shou, W., Chien, K.R., 2004. Nkx2–5 pathways and congenital heart disease; loss of ventricular myocyte lineage specification leads to progressive cardiomyopathy and complete heart block. Cell 117, 373–386.

Pasumarthi, K.B., Nakajima, H., Nakajima, H.O., Jing, S., Field, L.J., 2000. Enhanced cardiomyocyte DNA synthesis during myocardial hypertrophy in mice expressing a modified TSC2 transgene. Circ. Res. 86, 1069–1077.

Postlethwait, J.H., Talbot, W.S., 1997. Zebrafish genomics: from mutants to genes. Trends Genet. 13, 183–190.

Ransom, J., Srivastava, D., 2007. The genetics of cardiac birth defects. Semin. Cell Dev. Biol. 18, 132–139.

Rottbauer, W., Baker, K., Wo, Z.G., Mohideen, M.A., Cantiello, H.F., Fishman, M.C., 2001. Growth and function of the embryonic heart depend upon the cardiac-specific L-type calcium channel alpha1 subunit. Dev. Cell 1, 265–275.

Rottbauer, W., Saurin, A.J., Lickert, H., Shen, X., Burns, C.G., Wo, Z.G., Kemler, R., Kingston, R., Wu, C., Fishman, M., 2002. Reptin and pontin antagonistically regulate heart growth in zebrafish embryos. Cell 111, 661–672.

Rottbauer, W., Wessels, G., Dahme, T., Just, S., Trano, N., Hassel, D., Burns, C.G., Katus, H. A., Fishman, M.C., 2006. Cardiac myosin light chain-2: a novel essential component of thick-myofilament assembly and contractility of the heart. Circ. Res. 99, 323–331.

Sakamoto, D., Kudo, H., Inohaya, K., Yokoi, H., Narita, T., Naruse, K., Mitani, H., Araki, K., Shima, A., Ishikawa, Y., Imai, Y., Kudo, A., 2004. A mutation in the gene for delta-aminolevulinic acid dehydratase (ALAD) causes hypochromic anemia in the medaka, *Oryzias latipes*. Mech. Dev. 121, 747–752.

Sehnert, A.J., Huq, A., Weinstein, B.M., Walker, C., Fishman, M., Stainier, D.Y., 2002. Cardiac troponin T is essential in sarcomere assembly and cardiac contractility. Nat. Genet. 31, 106–110.

Sheikh, F., Fandrich, R.R., Kardami, E., Cattini, P.A., 1999. Overexpression of long or short FGFR-1 results in FGF-2-mediated proliferation in neonatal cardiac myocyte cultures. Cardiovasc. Res. 42, 696–705.

Soonpaa, M.H., Field, L.J., 1997. Assessment of cardiomyocyte DNA synthesis in normal and injured adult mouse hearts. Am. J. Physiol. 272, H220–226.

Soufan, A.T., van den Berg, G., Ruijter, J.M., de Boer, P.A., van den Hoff, M.J., Moorman, A.F., 2006. Regionalized sequence of myocardial cell growth and proliferation characterizes early chamber formation. Circ. Res. 99, 545–552.

Stuckmann, I., Evans, S., Lassar, A.B., 2003. Erythropoietin and retinoic acid, secreted from the epicardium, are required for cardiac myocyte proliferation. Dev. Biol. 255, 334–349.

Sultana, N., Nag, K., Hoshijima, K., Laird, D.W., Kawakami, A., Hirose, S., 2008. Zebrafish early cardiac connexin, Cx36.7/Ecx, regulates myofibril orientation and heart morphogenesis by establishing Nkx2.5 expression. Proc. Natl. Acad. Sci. U. S. A. 105, 4763–4768.

Thisse, C., Thisse, B., 2008. High-resolution in situ hybridization to whole-mount zebrafish embryos. Nat. Protoc. 3, 59–69.

Tokola, H., Hautala, N., Marttila, M., Magga, J., Pikkarainen, S., Kerkela, R., Vuolteenaho, O., Ruskoaho, H., 2001. Mechanical load-induced alterations in B-type natriuretic peptide gene expression. Can. J. Physiol. Pharmacol. 79, 646–653.

Toyoda, M., Shirato, H., Nakajima, K., Kojima, M., Takahashi, M., Kubota, M., Suzuki-Migishima, R., Motegi, Y., Yokoyama, M., Takeuchi, T., 2003. jumonji down-regulates cardiac cell proliferation by repressing cyclin D1 expression. Dev. Cell 5, 85–97.

Wills, A.A., Holdway, J.E., Major, R.J., Poss, K.D., 2008. Regulated addition of new myocardial and epicardial cells fosters homeostatic cardiac growth and maintenance in adult zebrafish. Development 135, 183–192.

Xu, X., Meiler, S.E., Zhong, T.P., Mohideen, M., Crossley, D.A., Burggren, W.W., Fishman, M.C., 2002. Cardiomyopathy in zebrafish due to mutation in an alternatively spliced exon of titin. Nat. Genet. 30, 205–209.

Yoshinari, N., Ishida, T., Kudo, A., Kawakami, A., 2009. Gene expression and functional analysis of zebrafish larval fin fold regeneration. Dev. Biol. 325, 71–81.

EXPERIMENTAL and MOLECULAR MEDICINE, Vol. 42, No. 3, 155-165, March 2010

Strategies for ensuring that regenerative cardiomyocytes function properly and in cooperation with the host myocardium

Fumiyuki Hattori[1,2,3] and Keiichi Fukuda[1,3]

[1]Division of Cardiology
Department of Medicine
Keio University School of Medicine
Tokyo, Japan
[2]Asubio Pharma Co., Ltd.,
Osaka, Japan
[3]Corresponding authors: E-mail, hattori@sc.itc.keio.ac.jp (F.H.);
E-mail, kfukuda@sc.itc.keio.ac.jp (K.F.)
DOI 10.3858/emm.2010.42.3.022

Accepted 25 January 2010
Available Online 11 February 2010

Abbreviations: EGFP, enhanced green fluorescent protein; EPC, endothelial progenitor cell; ES cells, embryonic stem cells; iPS cells, induced pluripotent stem cells

Abstract

In developed countries, in which people have nutrient-rich diets, convenient environments, and access to numerous medications, the disease paradigm has changed. Nowadays, heart failure is one of the major causes of death. In spite of this, the therapeutic efficacies of medications are generally unsatisfactory. Although whole heart transplantation is ideal for younger patients with heart failure, many patients are deemed to be unsuitable for this type of surgery due to complications and/or age. The need for therapeutic alternatives to heart transplantation is great. Regenerative therapy is a strong option. For this purpose, several cell sources have been investigated, including intrinsic adult stem or progenitor cells and extrinsic pluripotent stem cells. Most intrinsic stem cells seem to contribute to a regenerative environment *via* paracrine factors and/or angiogenesis, whereas extrinsic pluripotent stem cells are unlimited sources of cardiomyocytes. In this review, we summarize the various strategies for using regenerative cardiomyocytes including our recent progressions: non-genetic approaches for the purification of cardiomyocytes and efficient transplantation. We expect that use of intrinsic and extrinsic stem cells in combination will enhance therapeutic effectiveness.

Keywords: embryonic stem cells; guided tissue regeneration; heart; induced pluripotent stem cells; myocytes, cardiac; transplants

Introduction

The heart is designed as a blood pump that works from the earliest organogenetic stage until death. Cardiomyocytes lose the ability to undergo cytokinesis soon after birth, which means that instead they hypertrophy in line with the increased demand for blood supply; which may be an evolutionary strategy to avoid tumorigenesis and achieve long-term stable and high-power pumping functions. However, once a certain number of cardiomyocytes is lost, the functional loss is compensated by pathological hypertrophic remodeling of the remaining cardiomyocytes, which have limited capacity. The excessive remodeling and overload of cardiomyocytes causes their sequential death and an irreversible circle of degeneration.

Although whole heart transplantation is the optimal treatment for a severely failing heart, the numbers of donor hearts are limited. Furthermore, many patients who suffer heart failure are excluded from transplantation therapy due to complications and/or age. Therefore, revolutionary therapeutic alternatives to heart transplantation that can be applied to patients with general congestive heart failure are urgently needed. Heart regenerative therapy is a strong candidate for this type of therapy.

For the proper regeneration of heart functions, it is necessary to have a clear understanding of the nature of this organ. The heart is a complex organ that consists of various types of cells, including cardiomyocytes and non-cardiomyocytes. Cardiomyocytes can be categorized as atrial, ventricular, pacemaking, and purkinje. Furthermore, ventricular cardiomyocytes are functionary sub-divided into M-cell, sub-endocardial, and sub-epicardial cardiomyocytes. Non-cardiomyocytes include fibroblasts, endocardial and epicardial cells, vascular endothelial and smooth muscle cells, sympathetic and parasympathetic cells, valvular and chordal cells, and cardiac-resident immune cells. These cell types work co-operatively to create the physiologic heart. Therefore, to ensure that regenerative cardiomyocytes function properly, provision of the appropriate regenerative environment is critical.

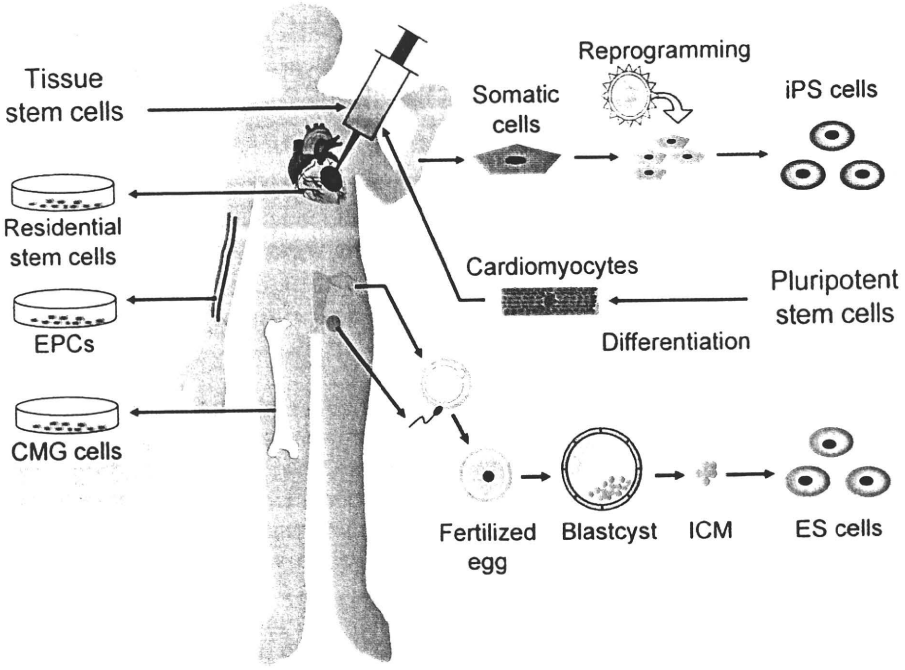

Figure 1. Sources of cells for regenerative therapies.

There are many candidate cell sources for heart regenerative therapies, such as cardiac-resident, bone marrow, and peripheral blood-derived stem cells. However, no adult stem cell-based strategy has achieved the production of sufficient numbers of cardiomyocytes to enable functional recovery of the failing heart. It is clear that the primary role of some adult stem cells is the creation of the regenerative environment rather than regeneration of cardiomyocytes. Therefore, cardiomyocyte administration/substitution from outside sources, e.g., human embryonic and induced pluripotent stem cells, appears to be promising (Figure 1).

In the present report, we introduce strategies for the preparation and delivery into the host myocardium of stem cells. The ultimate goal is to ensure that regenerative cardiomyocytes work properly and co-operatively with the host myocardium. Although different strategies are being tested, we believe that these studies will generate safe and effective therapies in the future.

Selection of cell sources

Tissue stem cells

In 1999, we demonstrated that bone marrow mesenchymal stem cells, which we term cardiomyogenesis cells, transdifferentiated into cardiomyocytes after treatment with 5-azacytidine (Makino *et al.*, 1999). This finding and previously obtained information on heart-derived cardiomyocytes (Soonpaa *et al.*, 1994) ushered in the concept of "heart regeneration therapies with own cardiogenic stem cells". Furthermore, we demonstrated the transplantation of cardiomyogenesis cells into the heart and observed that the integrated cardiomyogenesis cells had features of the adult myocardium (Hattan *et al.*, 2005). However, the cardiomyogenesis-based therapy has two major drawbacks: (1) the need to use the teratogenic reagent 5-azacytidine; and (2) low efficiency in terms of the establishment of cardiogenic cell lines from primary cultures of bone marrow adhesive cells. Despite intensive investigations, we have not yet overcome these obstacles.

5-Azacytidine is known to be an inhibitor of DNA methyltransferase (Kiefer, 2007). Recent publications have revealed the relationships between epigenetic modifications and the developmental specification of cell fates (Kiefer, 2007). In this context, we believe that cardiomyogenesis cells represent dedifferentiated cardiogenic stem cells. Other stem cells that have been identified for cardiomyocyte generation include endothelial progenitor cells (EPCs) (Asahara, 2007), c-kit (Beltrami *et al.*, 2003), sca-1 (Oh *et al.*, 2004), isl-1 (Laugwitz *et al.*, 2005), and neural crest stem cells (Tomita *et al.*, 2005). Asahara's group first reported the existence in the peripheral blood of multipotent stem cells, which are recruited into injured tissues and contribute to healing. They showed that EPCs not only differentiate into vessel endothelial and smooth muscle cells, but also cardiomyocytes,

albeit with very low efficiency. The c-kit-positive cells were identified as residential stem cells by Anversa's group (Beltrami *et al.*, 2003); these cells can repopulate cardiomyocytes under both normal and pathologic conditions. They reported that transplantation of collected and concentrated c-kit-positive cells dramatically improved cardiac function and inhibited remodeling. Moreover, they developed a method for expanding c-kit-positive stem cells *in vitro* (Beltrami *et al.*, 2003). The cardiogenic potential of sca-1-positive stem cells was first reported by Oh and colleagues (Oh *et al.*, 2004). These authors showed that sca-1-positive cells have high telomerase activity and can be differentiated into cardiomyocytes *in vitro* through treatment with 5-azacytidine. They also indicated that sca-1-positive cells have the potential to promote regenerative healing *in vivo* through both fusion and non-fusion cardiogenic transdifferentiation mechanisms.

Isl1 cells were discovered as cardiac-lineage progenitor cells by Chien's group (Laugwitz *et al.*, 2005). They reported the expression of transcription factor Isl1 in secondary cardiogenic cells at the cardiac crescent stage. From lineage-tracing studies, Isl1-positive cells have been found to contribute to atrial and right ventricular construction. Few Isl1-positive cells are observed in the neonatal atrial right ventricular, and they are absent from the adult heart. Isl1-positive cells can be isolated from murine embryonic stem cells, and they can be expanded and differentiated into vascular endothelium, vascular smooth muscle, and cardiomyocytes. Tomita *et al.* (2005) have shown that mammalian neural crest-derived cells have the potential to differentiate into cardiomyocytes, and they regard neural crest stem cells as new residential multipotential progenitor cells.

Pluripotent stem cells

Embryonic stem cells: Embryonic stem (ES) cells can be produced from the blastocyst inner cell mass. Therefore, the production of human ES cells from embryos raises ethical concerns. This is the major drawback to the use of human ES cells for research and therapeutics. Differences in the differentiation abilities of several ES cell lines have been reported (Moore *et al.*, 2008). Some researchers have attributed this to differences in epigenetic modifications or the accumulation of certain mutations. Since the differentiation efficiencies are generally low, the enhancement of differentiation efficiency has been studied extensively. ES cells have the ability to produce teratomas upon transplantation into immunodeficient animals (Prokhorova *et al.*, 2008). Therefore, in applications involving cells differentiated from ES cells, undifferentiated ES cells and unwanted cells must be excluded. Some studies have reported the susceptibility of human ES cells to become 'cancer ES cells' through the accumulation of mutations and genomic rearrangements (Harrison *et al.*, 2007). Although ES cells can theoretically proliferate indefinitely, many researchers believe that ES cells that have undergone more than 30 passages should not be used even for research purposes. The methodologies used for culturing and expanding ES cells should be stringently verified with respect to genomic and epigenetic stability. For ES cells used in therapies, an animal cell-free culture system should be used. Recently, improved systems have been reported, and some of these are already commercially available.

Induced pluripotent stem (iPS) cells: Recently, Takahashi *et al.* revealed that induced pluripotent stem (iPS) cells could be generated not only in mice (Takahashi and Yamanaka, 2006), but also in humans (Takahashi *et al.*, 2007); this may allow us to obtain individual ES-like cells. In our hands, the established murine iPS and ES cells and human iPS and ES cells are similar in terms of cell morphology, stem cell marker expression, and teratoma formations. However, cardiogenic differentiation properties tend to be lower than ES cells. The greatest advantage of iPS cells for stem cell researchers is that they do not have the ethical issues of ES cells, as they are derived from non-embryonic sources, although there are many unrevealed cocerns in iPS cells.

Mass production of ES cell-derived cardiomyocytes

For the eventual application of ES/iPS cell-derived cardiomyocytes, there are two major prerequisites: 1) improvement of the efficiency of differentiation into cardiomyocytes; and 2) efficient mass production of the differentiated cells. Many attempts have been made to improve cardiogenic differentiation efficiencies (Wobus *et al.*, 1997; Sauer *et al.*, 2000; Pandur *et al.*, 2002; Paquin *et al.*, 2002; Choi *et al.*, 2004; Kanno *et al.*, 2004; Passier *et al.*, 2005; Stary *et al.*, 2005; Yuasa *et al.*, 2005; Zhu and Lou 2005; E *et al.*, 2006; Hosseinkhani *et al.*, 2007a, 2007b; Roggia *et al.*, 2007; Singh *et al.*, 2007). However, inter-species, inter-strain, inter-laboratory, and even intra-laboratory variabilities have been problematic, and differentiation efficiencies >30% (cell-based counting) have not been achieved